

The Design and Synthesis of Potent and Selective Inhibitors of *Trypanosoma brucei* Glycogen Synthase Kinase 3 for the Treatment of Human African Trypanosomiasis

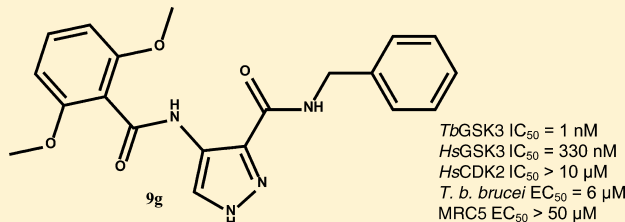
Robert Urich,[†] Raffaella Grimaldi,[†] Torsten Luksch,[†] Julie A. Frearson,[†] Ruth Brenk,^{*,‡,§} and Paul G. Wyatt^{*,†}

[†]Drug Discovery Unit, College of Life Sciences, University of Dundee, Sir James Black Centre, Dow Street, Dundee DD1 5EH, U.K.

[‡]Division of Biological Chemistry and Drug Discovery, College of Life Sciences, University of Dundee, Sir James Black Centre, Dundee DD1 5EH, U.K.

Supporting Information

ABSTRACT: Glycogen synthase kinase 3 (GSK3) is a genetically validated drug target for human African trypanosomiasis (HAT), also called African sleeping sickness. We report the synthesis and biological evaluation of aminopyrazole derivatives as *Trypanosoma brucei* GSK3 short inhibitors. Low nanomolar inhibitors, which had high selectivity over the off-target human CDK2 and good selectivity over human GSK3 β enzyme, have been prepared. These potent kinase inhibitors demonstrated low micromolar levels of inhibition of the *Trypanosoma brucei brucei* parasite grown in culture.



INTRODUCTION

Human African trypanosomiasis (HAT) or African sleeping sickness is a serious life threatening disease.¹ Around 60 million people in 36 African countries are currently in constant threat of infection. Although the reported number of cases has dropped over recent years, the actual number of unreported cases is estimated to be around 70000–80000.² HAT is caused by infection with *Trypanosoma brucei*, a vector-borne parasite, which is transmitted by the bite of tsetse flies. The symptoms of the disease occur in two main stages. In the first stage, known as the hemolymphatic phase, the parasites multiply in blood, subcutaneous tissues, and lymph, causing headaches, fever, itching, joint pains, and swelling of lymph nodes. In the second stage, or neurological phase, the trypanosomes cross the blood–brain barrier and invade the central nervous system. This phase entails confusion, change of behavior, reduced coordination, sensory disturbances, disturbance of sleep cycle, and finally death. Most available drugs for HAT display severe toxic side effects, require long periods of administration, and/or are expensive due to the logistics to reach rural African areas.³ Further, resistance to all in use drugs has been observed in the laboratory and/or in the field,⁴ resulting in an urgent requirement for better, safer, and inexpensive therapeutic alternatives to the current treatments.

Genetic knockdown studies have identified several proteins that are essential for the survival of the parasite, including members of the protein kinase (PK) family.^{5–8} In *Trypanosoma brucei* PKs are essential in many fundamental cellular processes, e.g., proliferation, differentiation, and cell cycle control, and can

therefore be considered as potential drug targets for the treatment of HAT.^{7,9–12}

In the *T. brucei* genome there are two kinases that are highly homologous to human glycogen synthase kinase 3 (*HsGSK3*): *TbGSK3* short and *TbGSK3* long.¹³ RNA interference (RNAi) knockdown of *TbGSK3* has shown that *TbGSK3* short is critical for cell growth, with a role in the control of mitosis and/or cytokinesis.^{7,13}

The ability to selectively inhibit *TbGSK3* over the off-target *HsGSK3* is highly desirable because mouse knockout studies revealed that the disruption of the murine GSK3 β gene causes embryonic lethality; consequently, nonselective inhibitors are not applicable for use in infants and women of child bearing age.^{14,15}

From a homology perspective, *TbGSK3* is not only very closely related to *HsGSK3 β* but also to other human PKs such as cyclin dependent kinase 1 (*HsCDK1*) and cyclin dependent kinase 2 (*HsCDK2*).¹⁶ *HsCDK2* and *HsCDK1* are essential for G1/G2 progression and S/M-phase entry of the cell cycle. Off-target inhibition of these human kinases will therefore result in cell cycle arrest and reduction of cellular proliferation and as such potentially lead to severe side effects.

Over the past decade, various groups and pharmaceutical companies have identified multiple series of *HsGSK3 β* inhibitors.^{16,17} Recently, Astex Therapeutics and researchers at the University of Osaka have developed a series of aminopyrazoles that are potent inhibitors of *HsGSK3 β .*^{18–20}

Received: February 13, 2014

Published: September 8, 2014

Co-crystal structures of this series with *HsGSK3β* are not available to date; however, complex structures with the closely related *HsCDK2* have been determined.¹⁹ In all structures, the pyrazole scaffold forms two hydrogen bonds to the hinge region of *HsCDK2* (Figure 1). Further, the NH group of the 3-

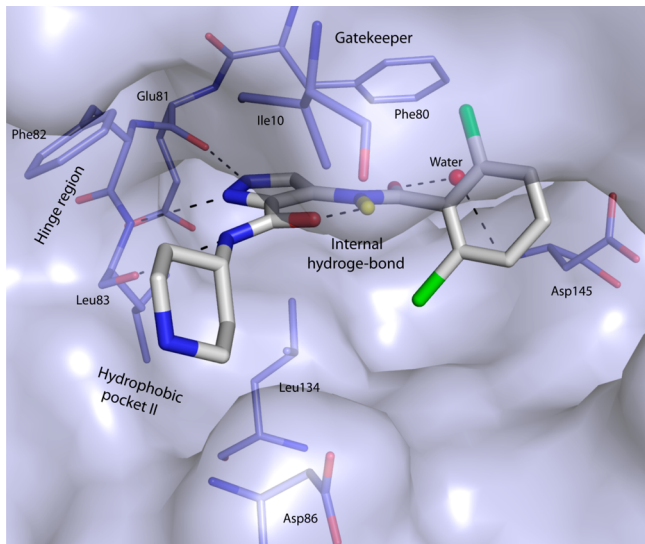


Figure 1. Co-crystal structure (2vu3)¹⁹ (carbon atoms in gray) bound to CDK2. The binding pocket of CDK2 is shown in light-blue surface representation. Key: red sphere, water molecule; black dashed lines, protein–ligand and water–ligand hydrogen bonds; yellow stick, hydrogen atom..

position amide forms an additional hydrogen-bond interaction to the backbone of Leu83. A water-mediated hydrogen bond from the amide carbonyl oxygen atom to the backbone NH of Asp145 is also observed. The R¹ residues (Figure 2) access the

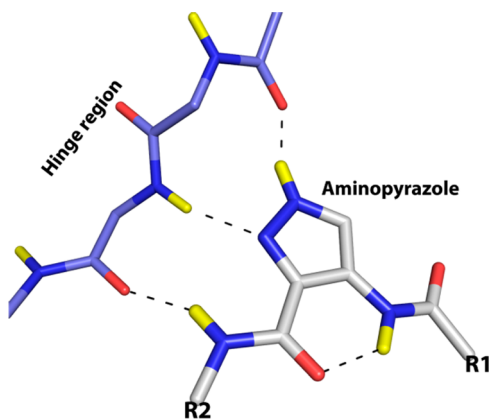


Figure 2. Generic binding mode of the R¹ and R² substituted aminopyrazole scaffold (carbon atoms in gray).

gatekeeper region between the gatekeeper residue Phe80 and the catalytic Asp145 (Figure 1). The R² substituents occupy the hydrophobic pocket II, formed by the backbone of the linker region, Leu83, Phe82, and side chains of Ile10, Asp86, and Leu134. Finally, an intramolecular hydrogen bond between the R¹-NH and R²-carbonyl group is present. The similarity of *HsCDK2*, *HsGSK3β*, and *TbGSK3* indicates that aminopyrazoles will also bind into the ATP-binding site of the latter enzyme.^{13,16}

Herein, we describe the design, synthesis, and biological evaluation of aminopyrazole inhibitors which bind to *TbGSK3* short. The inhibitors were also tested against the closely related off-targets *HsGSK3β* and *HsCDK2* and evaluated against a panel of mammalian protein kinases. The most potent compound has nanomolar affinity for *TbGSK3* short, is selective over *HsGSK3β* and *HsCDK2*, and clean in the kinase panel. By using computer-aided molecular modeling, we were able to rationalize the observed selectivity profile. Enzyme affinity correlated with inhibition of *T. b. brucei* proliferation, albeit a 100-fold offset in potency, was found. In light of these results, we discuss the value of *TbGSK3* short as a drug target for HAT.

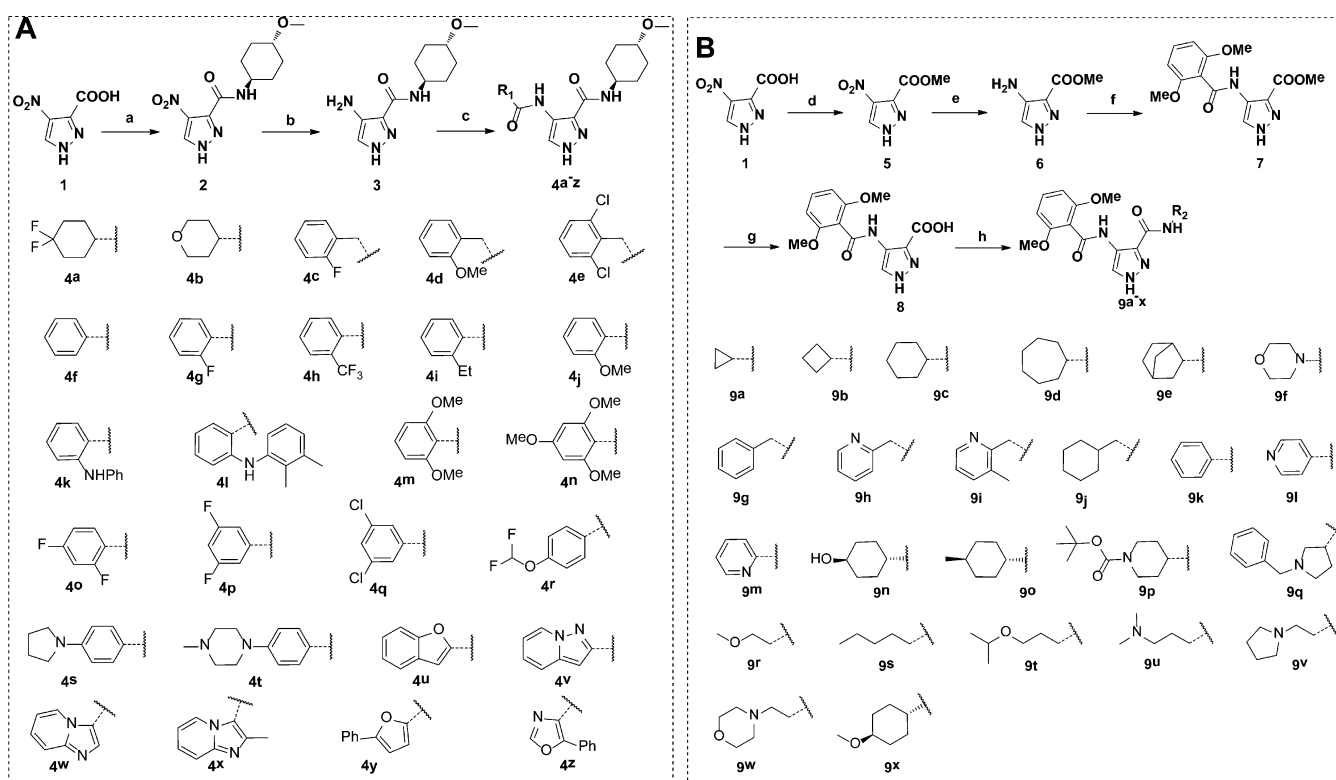
RESULTS

Starting Point. The aminopyrazole derivatives developed by Astex Therapeutics and Yumiko Uno et al. for inhibition of *HsCDK2* and *HsGSK3β* enzymes were chosen as a starting point for the investigation of *TbGSK3* short inhibitors.^{18–20} Aminopyrazoles analogues were generated by substituting at either R¹ or R² position (Figure 2) using two synthetic routes (Scheme 1A,B).

Differences in the ATP Binding Pockets of *TbGSK3*, *HsGSK3β*, and *HsCDK2*. A structural model of *TbGSK3* was built to assess the differences in the binding sites of *TbGSK3* short, *HsGSK3β*, and *HsCDK2* and to guide ligand design. An overlay of 42 *HsGSK3* crystal structures showed that there is low flexibility in the ATP binding site. Only the regions including Phe67 and Arg141 showed some mobility. Phe67 either points toward or away from the hinge region. Arg141 also spans a number of distinct conformations, including examples where it occupies space in the binding site (1J1B, 1J1C, 1O9U, 2OSK) and therefore could influence docking results. However, to allow for ligands of a significant size, we have used examples with Arg141 pointing out of the binding site. Therefore, two homology models for *TbGSK3* were generated representing both states of Phe67. As we were mainly interested in aminopyrazoles with less extended R¹ groups, the crystal structure with Phe67 pointing toward the hinge (with structure 1r0e as a representative) was more suited as model system. The selection of 1r0e instead of other members of this group (with Phe67 pointing toward the hinge) was arbitrary. For this analysis, all residues that are located within 6 Å of the ligand bound to the template structure (1r0e) were considered.

The binding pockets of *TbGSK3* and *HsGSK3β* differ by nine amino acid residues (Table 1, Figure 3A). Of the amino acid side chains that point toward the ligand, the most significant differences are the replacement of Tyr134 in *HsGSK3β* with Phe103, Leu132 with Met101, Gln72 with Leu36, and Tyr140 with His109. The binding pockets of *TbGSK3* and *HsCDK2* are more diverse. Here, in total 16 out of 26 amino acids were found to be different (Table 1, Figure 3B), the most important of these differences being the replacement of Lys20 in CDK2 with Leu36, Phe80 with Met101, His84 with Pro105, Lys89 with Arg110, and Ala144 with Cys170. Interestingly, most of the amino acid differences occurred in the hydrophobic pocket II and the gatekeeper region. Therefore, we decided to direct the optimization of the lead scaffold toward suitable interactions with amino acids which are located in these subpockets of the ATP binding site.

Chemistry. The synthesis of R¹ and R² substituted aminopyrazole derivatives started from 4-nitro-pyrazole-3-carboxylic acid **1** and is described by two different routes

Scheme 1. Synthetic Routes for 50 R¹ and R² Substituted Aminopyrazoles (4a–z and 9a–x)^a

^aReagents and conditions used in routes A and B: (a) *trans*-4-methoxycyclohexylamine, EDC, HOBr, DMF, rt; (b) 10% Pd/C, H₂, DMF, rt; (c) R¹COOH, EDC, HOBr, DIPEA, rt; (d) SOCl₂, MeOH, 0°C, rt; (e) 10% Pd/C, H₂, EtOH, rt; (f) 2,6-dimethoxybenzoylchloride, Et₃N, dioxane, rt; (g) NaOH, dioxane, H₂O, rt; (h) R₂NH₂, polystyrene-bound carbodiimide, HOBr, acetonitrile, MW, 100 °C.

(Scheme 1) based on previous work from Wyatt et al.¹⁹ In route A, 1 was coupled with *trans*-4-methoxycyclohexylamine using EDC as the activating agent. Reduction of the subsequent intermediate 2 by hydrogenation in the presence of palladium on carbon generated amino pyrazole 3. The conversion to compounds 4a–z was accomplished by coupling of 3 with a suitable selection of carboxylic acids. In route B, after esterification of the carboxyl group of 1, the nitro group of intermediate 5 was reduced to afford amine 6. Treatment of 6 with 2,6-dimethoxybenzoyl chloride under standard conditions, followed by base hydrolysis of the ester, provided acid 8. In the final step, 8 was coupled with appropriate amines in a microwave reaction using polystyrene-bound carbodiimide to yield final compounds 9a–x.

Activity and Selectivity of R¹ Substituted Compounds. Twenty-six R¹ substituted aminopyrazole analogues (Table 2) were made according to the synthetic route shown in Scheme 1A. A range of R¹ groups varying in size and polarity was chosen to probe whether the differences in the gate keeper region between *TbGSK3*, *HsGSK3*, and *HsCDK2* could be exploited to derive selective and potent *TbGSK3* inhibitors (Figure 3).

Enzyme Activity. All compounds showed good potency against *TbGSK3* (<1 μM). An unsubstituted phenyl ring (4f) provided on average a 20-fold improvement of inhibition potency relative to saturated six-membered ring systems (4a and 4b) and benzyl groups (4c, 4d, and 4e). In general, a variety of different aryl and heteroaryl rings (4g–4y compared to 4a and 4b) in the R¹ position led to significantly improved potency against *TbGSK3*. Additionally, a wide variety of

substituents were tolerated on the phenyl ring. In general, *ortho*-substituted phenyl rings gave the best improvement in activity compared to the unsubstituted phenyl group (4j, 4k, 4m, and 4n). The methoxyphenyl moieties in 4j, 4m, and 4n, which had *TbGSK3* IC₅₀ values of 4, 2, and 3 nM, respectively, were the most favorable substituents. These derivatives were approximately 10-fold more potent than the unsubstituted phenyl compound 4f. Only the 2,4,6-trimethoxy derivative 4n showed >10-fold selectivity over *HsGSK3*. Interestingly, this was also the most selective compound for *HsCDK2* (>1000-fold).

To rationalize the observed selectivity, all analogues were docked into the binding sites of *TbGSK3*, *HsGSK3β*, and *HsCDK2* and their poses were visually analyzed. For most compounds, a binding mode similar to that observed for AT7519¹⁹ in *HsCDK2* (Figure 1) was predicted in *TbGSK3*, *HsGSK3β*, and *HsCDK2*. One important difference between *HsCDK2*, *TbGSK3*, and *HsGSK3β* is the gatekeeper residue (Table 1, Figure 3A,B). While *HsGSK3* and *TbGSK3* enzymes have Leu or Met, respectively, in this position, in *HsCDK2* Phe is present. As a consequence, the gatekeeper region of *HsCDK2* (located between Phe80 and Asp145) is more restricted compared to the other two enzymes. This resulted in a higher energy, out of plane conformation of the amide group of 4f when binding into this pocket (Figure 4), while a low energy conformation was found when binding into *T. brucei* and human GSK3 (not shown). Further, without induced fit adaptations, the bulky R¹-substituents such as the 2,6-dimethoxybenzamide group of 4m, the 2,4,6-trimethoxybenzamide groups of 4n, and the phenylaminobenzamide groups of 4k

Table 1. Differences in the Binding Pockets of *TbGSK3*, *HsGSK3 β* , and *HsCDK2*^a

<i>TbGSK3</i>	<i>HsGSK3β</i>	<i>HsCDK2</i>
V25	V61	K9
A26	I62	I10
G27	G63	G11
Q28	N64	E12
G29	G65	G13
T30	S66	T14
F31	F67	Y15
V34	V70	V18
L36	Q72	K20
A47	A83	A31
K49	K85	K33
E61	E97	I52
M65	M101	L55
V77	V110	V64
M101	L132	F80
E102	D133	E81
F103	Y134	F82
104	V135	L83
P105	P136	H84
E106	E137	Q85
T107	T138	D86
H109	Y140	K88
R110	R141	K89
K154	K183	K129
H156	Q185	Q131
N157	N186	N132
L159	L188	L134
C170	C199	A144
D171	D200	D145

^aAmino acids of *hGSK3 β* or *HsCDK2* which differ in *TbGSK3* short are shown in boldface.

and **4l** can only be accommodated by the gatekeeper region of *TbGSK3* and *HsGSK3 β* but not the narrower *HsCDK2* gatekeeper region. These observations might explain the reduced binding affinity of **4f** for *HsCDK2* compared to *HsGSK3*. Of note, this explanation is further supported by the report by Wyatt et al.,¹⁹ which found that the aryl groups which are located in the same position need to twist in order to provide potent CDK2 activity.

Antiparasitic Activity. All R¹ substituted compounds were tested for their ability to inhibit the proliferation of bloodstream form (BSF) *T. b. brucei* in culture. As an initial indication of potential toxicity, compounds **4a–4z** were additionally tested against proliferating human fetal lung fibroblast cells (MRC5 cell line). Four compounds (**4g**, **4j**, **4m**, and **4y**) had EC₅₀ values <1 μ M and a further 11 compounds had EC₅₀ values <3 μ M against BSF *T. b. brucei* (Table 2). The EC₅₀ values correlated well with enzyme activity ($R^2 = 0.73$, Figure 5). However, a 100-fold drop from enzyme to cellular activity was observed. Selectivity over the MRC5 cells was achieved with compounds **4m** (60-fold), **4s** (>19-fold), **4x** (12-fold), and **4n** (>9-fold), however, the majority of compounds showed a poor selectivity over MRC5 cells.

Activity and Selectivity of R² Substituted Compounds. As **4m** was the most potent inhibitor of *TbGSK3* and proliferation of *T. b. brucei* cells, we retained the 2,6-dimethoxybenzamide group at position R¹ for optimization of the R² substituent. R² substituted aminopyrazole analogues (**9a–9x**) were made according to the synthetic route shown in Scheme 1B to explore the structural requirements for improvement of antiparasitic activity and selectivity over the closely related human kinases.

Enzyme Activity. The majority of variations led to potent *TbGSK3* inhibitors, indicating that chemical diversity at this position was well tolerated (Table 3). One of the SAR trends observed was that six-membered saturated rings (**9c**) and seven-membered saturated rings (**9d**) were favored over their three- and four-membered equivalents (**9a** and **9b**). Further, it

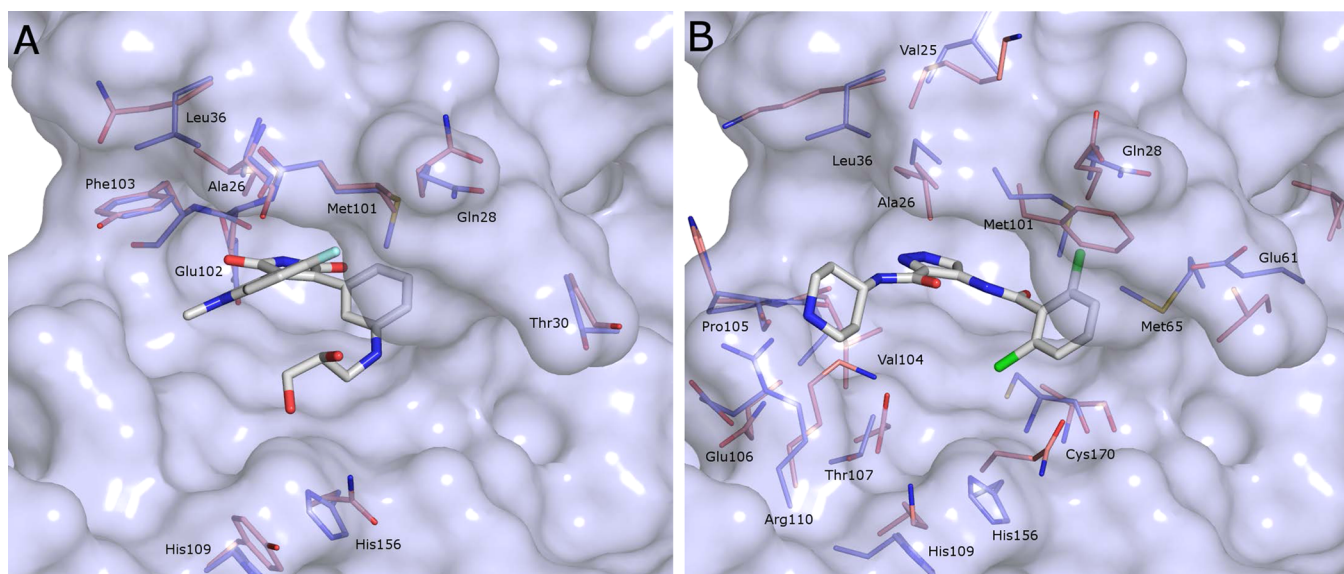


Figure 3. Superposition of the binding sites of the homology model of *TbGSK3* short (blue carbon atoms) with (A) the *HsGSK3 β* crystal structure (PDB code 1r0e) and (B) the *HsCDK2* crystal structure (PDB code 2vu3). The solvent accessible surface of *TbGSK3* short is shown in light blue. Only residues that differ between the binding pockets are shown. For orientation, the ligands bound to crystal structures are also displayed. Amino acid residue labels are for *TbGSK3*.

Table 2. Kinase Inhibitory Activity and Antiproliferative Efficacy of R¹ Substituted Aminopyrazoles

compd	IC ₅₀ (μ M)	IC ₅₀ (μ M)	IC ₅₀ (μ M)			EC ₅₀ (μ M)	
	TbGSK3 ^a	HsGSK3 β ^a	ratio HsGSK3 β /TbGSK3	HsCDK2 ^a	ratio HsCDK2/TbGSK3	T. b. brucei ^b	MRC5 ^c
4a	0.50	0.008	0.16	1.0	2	16	>50
4b	0.69	0.008	0.0012	0.38	0.55	32	>50
4c	0.39	0.14	0.35	0.82	2.1	23	>50
4d	0.50	0.21	0.42	0.85	1.7	22	40
4e	0.23	0.2	0.87	0.29	1.3	7.3	3.1
4f	0.024	<0.005	>0.21	0.038	<1.6	1.3	0.8
4g	0.020	<0.005	0.25	0.014	<0.7	0.4	1.0
4h	0.018	<0.013	<0.72	0.1	5.6	2.3	3.3
4i	0.053	0.02	0.38	0.07	1.3	2.8	3.4
4j	0.004	<0.013	<3.3	0.1	25	0.9	1.5
4k	0.011	0.02	1.8	>10	>910	4.4	35
4l	0.066	0.03	0.45	>10	>150	5.8	16
4m	0.002	<0.005	<2.5	0.19	95	0.5	31
4n	0.003	0.09	30	3.1	1000	5.9	>50
4o	0.053	<0.005	<0.09	0.22	4.2	3.8	11
4p	0.024	<0.005	<0.21	0.083	3.5	2.6	0.6
4q	0.057	<0.005	<0.08	0.63	11	9.6	13
4r	0.016	<0.005	<0.31	0.27	17	1.1	2.5
4s	0.019	<0.005	<0.26	0.13	6.8	2.7	>50
4t	0.070	<0.005	<0.071	1.0	14	2.0	20
4u	0.013	<0.005	<0.38	nd	nd	1.2	0.8
4v	0.063	<0.005	<0.080	0.042	0.67	1.9	1.0
4w	0.094	<0.005	<0.053	0.15	1.6	2.6	5.9
4x	0.10	0.042	0.42	2.2	22	2.9	34
4y	0.007	<0.005	<0.72	0.01	1.4	0.3	0.1
4z	0.92	0.005	0.0058	22	24	>50	28

^aData represents the average of two or more experiments. ^bConcentration required to inhibit the growth of *T. b. brucei* in culture by 50% over 72 h.

^cConcentration required to inhibit the growth of MRC5 cells in culture by 50% over 72 h.

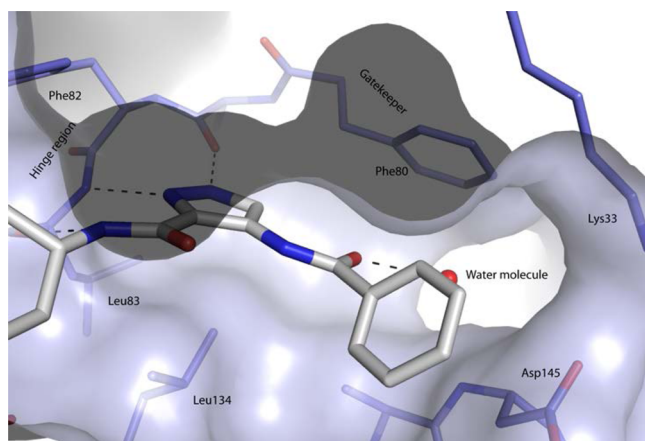


Figure 4. Predicted binding mode of 4f in HsCDK2. Putative hydrogen bonds are shown as black dotted lines. Docking results suggested that the phenyl ring of compound 4f needs to be significantly twisted out of plane by approximately 60° compared to the amide in order to fit into the gatekeeper region.

was noted that the replacement of the cyclohexane of 9c with a phenyl ring or 4-pyridine, to give 9k or 9l, gave a 6-fold decrease in potency against TbGSK3. The 2-pyridine analogue (9m), on the other hand, was much less active (50-fold) against TbGSK3. Homologation of aromatic (9g) and saturated six-membered (9j) rings by one carbon atom produced inhibitors with 1 nM activity for TbGSK3. For aliphatic side chain derivatives 9r–9w, the pentanyl and 1-isopropoxypropanyl analogues had IC₅₀ values of 1 nM. The impact of replacing the

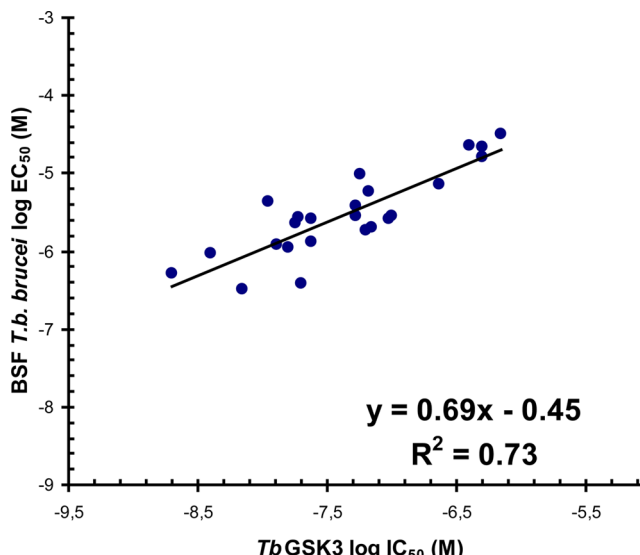


Figure 5. Correlation between the inhibition of recombinant TbGSK3 and bloodstream form *T. b. brucei* proliferation by R¹ substituted aminopyrazole derivatives (4a–z).

amide group (3-position) with carboxylic acid and ester groups was investigated with compounds 8 and 7. Compound 8 containing a carboxylate group in the 4-position showed a dramatic loss in activity (IC₅₀ >50 μ M). The ester group of compound 7 on the other hand was better tolerated (IC₅₀ 0.5 μ M). Interestingly, compared with 4a–4z, a majority of R² substituted analogues (9a–9x) showed selectivity over

Table 3. Kinase Inhibitory Activity and Antiproliferative Efficacy of R² Substituted Aminopyrazoles

compd	IC ₅₀ (μ M)	IC ₅₀ (μ M)	IC ₅₀ (μ M)				EC ₅₀ (μ M)	
	TbGSK3 ^a	HsGSK3 β ^a	ratio HsGSK3 β /TbGSK3	HsCDK2 ^a	ratio HsCDK2/TbGSK3	T. b. brucei ^b	MRC5 ^c	
9a	0.012	0.22	18	>10	>830	19	>50	
9b	0.008	0.08	10	2.4	300	12	>50	
9c	0.001	0.05	50	1.2	1200	4.1	35	
9d	0.001	0.02	20	2.0	2000	4.5	42	
9e	0.018	nd	nd	>10	560	16	>50	
9f	0.081	0.45	5.6	>10	120	50	>50	
9g	0.001	0.33	330	>10	10000	5.9	50	
9h	0.015	0.32	21	>10	670	20	>50	
9i	0.14	0.87	6.2	>10	71	>50	>50	
9j	0.001	nd	nd	nd	nd	7.7	>50	
9k	0.006	0.07	12	4.3	720	11.5	>50	
9l	0.004	0.12	30	1.3	330	8.2	>50	
9m	0.32	0.94	2.9	>10	31	>50	>50	
9n	0.002	0.07	35	1.6	800	6.4	34	
9o	0.001	nd	nd	>4.8	4800	6.7	45	
9p	0.006	0.14	23	4.7	780	12	>50	
9q	0.008	0.08	10	>10	1300	8.9	38	
9r	0.034	0.3	8.8	>10	290	43	>50	
9s	0.001	0.1	100	4.8	4800	7.3	>50	
9t	0.001	nd	nd	>10	10000	6.6	>50	
9u	0.33	0.47	1.4	>10	30	>50	>50	
9v	0.32	0.66	2.1	>10	31	>50	>50	
9w	0.054	0.63	12	>10	190	>50	>50	
9x	0.002	<0.005	<2.5	0.19	95	0.5	31	
8	>50	>10		>10		>50	>50	
7	0.52	4.5	8.7	>10	19	>50	>50	

^aData represents the average of two or more experiments. ^bConcentration required to inhibit the growth of *T. b. brucei* in culture by 50% over 72 h.

^cConcentration required to inhibit the growth of MRC5 cells in culture by 50% over 72 h.

HsCDK2 and HsGSK3 β . These are the most selective TbGSK3 inhibitors described to date.

The predicted binding mode of 9g in TbGSK3 offers an explanation for the observed selectivity (Figure 6). In the highest scoring docking pose, the core scaffold adopts a similar binding mode as observed for AT7519 in HsCDK2 (Figure 1).¹⁹ In addition, the docking results suggested that the hydrophobic pocket II of TbGSK3 was occupied by the N-benzylamide group of 9g in such a way that its phenyl moiety formed T-shaped edge-to-face interactions with the side chain of Phe103 and hydrophobic interactions with Leu36 and Ala26. In hGSK3 β , Phe103 is replaced with a Tyr (Table 1, Figure 3A), resulting in steric clash and electrostatic repulsion toward the benzyl moiety of 9g. Further, Leu36 is substituted with Gln72 in hGSK3 β and Lys20 in HsCDK2, diminishing hydrophobic interactions between the benzyl moiety of 9g and these residues. Overall, these changes together with differences in the gatekeeper region of HsCDK2 (see above) are likely to be responsible for the high selectivity of 9g for TbGSK3 over hGSK3 and HsCDK2. Similar observations regarding the R² group placement and selectivity were also made for compound 9h supporting this model.

Antiparasitic Activity. The R² substituted compounds were tested against BSF *T. b. brucei* and MRC5 cells. As for the R¹-substituted analogues, a good correlation between the EC₅₀ and IC₅₀ values and a 100-fold drop in activity between the biochemical and cell assay was observed (Figure 7). Compound 9c had an EC₅₀ for *T. b. brucei* of 4 μ M (Table 3). Limited selectivity (>7-fold) over MRC5 cells was achieved with compounds 9c, 9d, 9g, 9s, and 9t. It was found that the

compounds showed selective inhibition of TbGSK3 over HsGSK3 (>20-fold) and HsCDK2 (>1200-fold).

Human Kinase Selectivity Profile. PK inhibitors frequently inhibit multiple kinases, often leading to off-target toxic effects. To assess the selectivity of the aminopyrazole inhibitors, remaining activity at 10 μ M concentration was measured for compounds 4f, 4m, and 4y against a panel of 80 human PKs and for compound 9g against 124 human PKs. Compounds 4m and 9g were found to be highly specific (Table 4). Compound 4m inhibited only two PKs, namely GSK3 β and CDK2, at more than 80%. 9g showed activity against three PKs: GSK3 β , MAPKAP-K2, and MINK1 at more than 80%. Compound 4f was found to inhibit seven PKs and compound 4y 15 PKs by greater than 80% at 10 μ M.

DISCUSSION

In this work, we exploited the knowledge of the previously described aminopyrazoles inhibitors of HsCDK2 and HsGSK3 β ²⁰ to identify selective inhibitors of the TbGSK3 short isoform. This kinase has been shown using genetic manipulation studies to be essential for the survival of the *T. b. brucei* parasite.¹³ However, we wanted to confirm if antiparasitic activity could be gained using selective, small molecule inhibitors of TbGSK3. The ability to selectively inhibit TbGSK3 over HsGSK3 and HsCDK2 is essential to avoid potential side effects. Therefore, more than 50 aminopyrazole derivatives were synthesized and screened against TbGSK3, HsGSK3 β , HsCDK2, and proliferating *T. b. brucei* and human cells in culture.

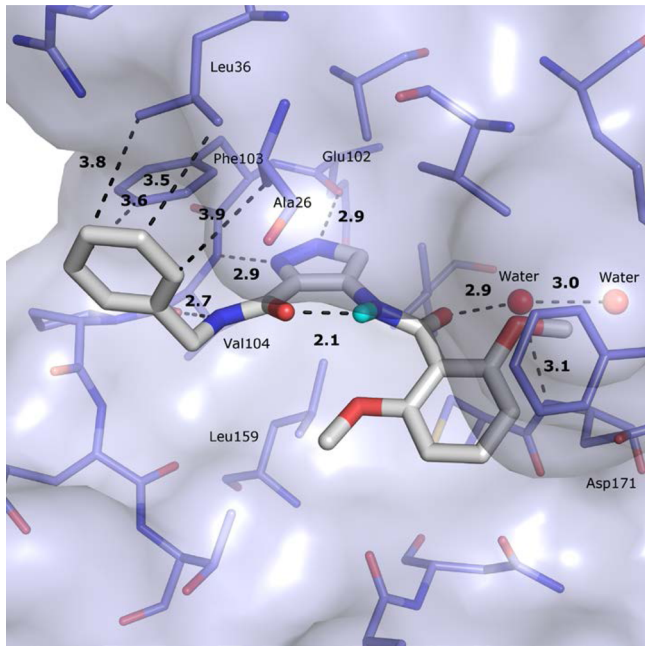


Figure 6. Proposed binding mode of **9g** in the homology model of TbGSK3 (blue carbon atoms) overlaid on the HsGSK3 β crystal structure (pink carbon atoms). Both ligand and protein are represented as sticks and color coded by atom types. Ligand carbon atoms are shown in gray, protein carbon atoms of TbGSK3 are shown in blue, and HsGSK3 β carbon atoms in salmon. Amino acid residue labels are for TbGSK3. Hydrogen bonds and hydrophobic interactions are shown as black dotted lines, with interaction distances in angstroms. TbGSK3 amino acids which are involved in hydrophobic interactions with the benzyl group are marked in bold. The gold sphere represents the center of the phenyl ring..

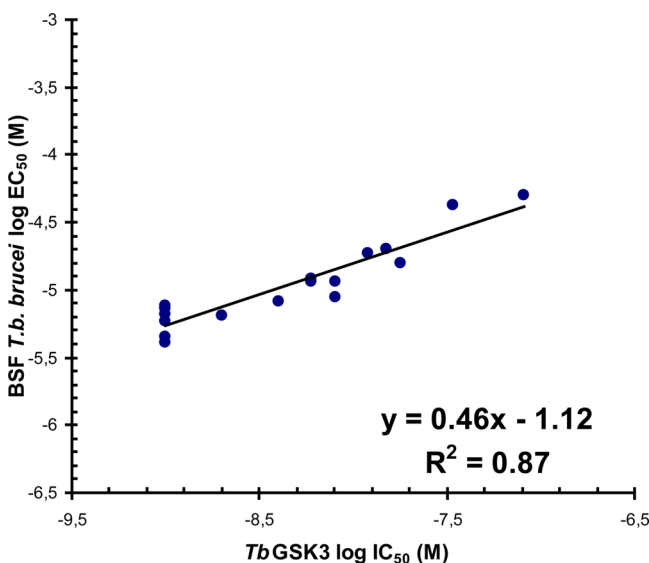


Figure 7. Correlation between the inhibition of recombinant TbGSK3 and bloodstream from *T. b. brucei* proliferation using R² substituted aminopyrazole derivatives (**9a–x**).

The results (Table 2 and Table 3) showed that almost all compounds were highly potent TbGSK3 inhibitors. The activity could be rationalized using the homology models and subsequent molecular docking studies (Figure 4 and Figure 6). The aminopyrazole derivatives make three H-bond interactions with the kinase hinge region, driving much of the

Table 4. Kinase Profiling against a Panel of Mammalian Kinases^a

PKs	4f	4m	4y	9g
MKK1	54	83	17	76
ERK2	18	51	2	92
JNK1	31	77	8	71
JNK2	51	82	15	63
ERK8	14	27	7	47
MAPKAP-K2	92	33	90	13
GSK3b	33	0	0	10
CDK2	1	9	1	38
MELK	32	100	13	96
DYRK1A	6	84	1	79
DYRK2	3	63	1	28
DYRK3	24	100	2	80
PIM1	46	100	13	92
PIM3	19	94	1	96
HIPK2	14	100	4	93
IGF-1R	96	100	15	79
MINK1	nd	nd	nd	18

^aNumbers represent average percentage of activity compared to the control at 10 μ M. In this table, only kinases with activity values <20% are shown (for full table see Supporting Information). PK activity values <20% are marked in bold.

potency of the compounds against the three kinases studied. Selectivity could be derived from substitution at both R¹ and R² positions.

From a homology perspective, HsCDK2 is the most closely related kinase to HsGSK3 β .¹⁶ Although, the enzymes only share approximately 33% amino acid identity, their ATP binding pockets are highly conserved,¹⁶ resulting in the majority of known HsCDK2 inhibitors also potently inhibiting HsGSK3 β . The results demonstrated that the required profile could be achieved, with several compounds with high affinity (<18 nM) for TbGSK3 showing high selectivity (>500-fold) over HsCDK2. Docking studies provided a number of important insights into the binding modes and the selectivity profile of aminopyrazole derivatives. First, the docking results suggested that if the phenyl ring of compound **4f** is planar with the amide group at R¹ position it cannot bind into the truncated gate keeper region of HsCDK2, defined by Phe80 in HsCDK2, compared to Met101 in TbGSK3. To fit into this region of HsCDK2, the phenyl ring needs to significantly twist out of plane of the amide, with a torsion angle of approximately 60°, resulting in reduced binding affinity (Figure 4). To stabilize this twist, di-ortho-substituents on the R¹ phenyl group are required to cause a steric/electronic clash with the carbonyl of the amide bond. However, this region of the pocket in HsCDK2 is narrow (in a plane perpendicular to the hinge backbone and the pyrazole core), only allowing small ortho-substituents (such as in compound **9g**) on the phenyl group. In contrast, the wider gatekeeper regions of hGSK3 and TbGSK3 can tolerate large substituents such as the ortho-dimethoxy groups of compound **4m** or **4n** and the ortho-phenylaminobenzamide groups of **4k** or **4l**. Second, the highest increase in selectivity (>10000-fold) over HsCDK2 was achieved by accessing the hydrophobic pocket II. Exploitation of hydrophobic interactions in these two pockets not only reliably increased ligand-binding affinity but also impacted on the selectivity profile of these compounds. On the basis of the biological results of compound **9g** and structural modeling studies, we have shown that selectivity over

HsGSK3 can be achieved by exploiting the Phe103Tyr, Leu36Gln, and Ala26Ile active site differences in the hydrophobic pocket II of *TbGSK3* enzyme (Figure 6). Taken together, the region between the gate keeper residue and the catalytic aspartate of the DFG loop, together with the hydrophobic pocket II, are the key areas to exploit to achieve high selectivity over *HsCDK2*.

The *TbGSK3* short enzyme IC_{50} values correlated well with the *T. b. brucei* antiproliferative EC_{50} activities of the described substituted aminopyrazole inhibitors (Figures 5 and 7), indicating that the compounds act on target. However, a 100-fold drop in cell activity was observed, compared to that in the *TbGSK3* assay ($1\ \mu M$). The calculated physical properties (MW < 473; log P –0.4–3.6; PSA < 130 Å) of the series of compounds suggest this loss of activity was not driven by lack of cellular penetration. In addition, the compound series was observed to be highly chemically stable under the range of synthetic conditions used during the chemistry campaign, suggesting that chemical degradation was not responsible for the loss of activity in the proliferation assay. Although metabolism by the parasite cannot be ruled out, the high degree of correlation between enzyme inhibition and antiparasitic activity suggests this is not the case, as it would be not expected that all compounds be metabolized to a constant extent. Therefore, the drop of activity was probably due to the high ATP concentration (millimolar range) in the cell compared to the kinase assay conditions.²¹ Furthermore, chemical proteomic profiling conducted in parasite cell extracts confirmed that compound **4m** binds the endogenous *TbGSK3* short with nanomolar affinity and very few other kinase targets with much lower affinity in the micromolar range.²²

CONCLUSION

In this study, we have developed a series of substituted aminopyrazole amides as *TbGSK3* short inhibitors starting from a compound series initially designed by Astex Therapeutics to inhibit *HsCDK2* and *HsGSK3β*. SAR investigation and optimization successfully provided 18 low nanomolar (IC_{50} < 10 nM) inhibitors of *TbGSK3* with high selectivity (>10000-fold) over *HsCDK2*. With compound **9g**, we have shown that good (330-fold) selectivity over *HsGSK3* can be achieved by targeting the hydrophobic pocket II. Compound **9g** is the most selective *TbGSK3* inhibitor described to date.^{13,23–25} In addition, **9g** proved to be highly selective against a panel of 124 human PKs, showing >90% inhibition at $10\ \mu M$ against only one PK, *HsGSK3β*. Molecular modeling has also shown that despite overall conservation in sequence and conformation between the three PKs (*HsGSK3β*, *HsCDK2*, and *TbGSK3*), the binding pockets have distinct features that determine their specificity for particular compounds. Further, we have shown that enzymatic inhibition correlates well with cell efficacy over a wide range of concentrations and a representative member of this series binds the endogenous *TbGSK3* with nanomolar potency, indicating that compounds definitely act on target.²² However, a general 100-fold drop in activity between target and cellular activities resulted at best in compounds with low micromolar antiparasitic activity. Taken together, this data suggests that specific ATP competitive hinge binders of *TbGSK3* short require low picomolar potency to obtain nanomolar antiproliferative activity against *T. brucei*. This leads us to the conclusion that alternative strategies are required. First, non-ATP competitive approaches to inhibition of *TbGSK3*, through

irreversible hinge binders or allosteric inhibitors, could be pursued. However, these approaches have potential downsides, through the introduction of a reactive functionality or an increased chance of resistance causing mutations, respectively. Second, a polypharmacology approach through the inhibition of a number of essential *T. brucei* kinases in addition to *TbGSK3* could be investigated, although obtaining selectivity over human kinases would be more problematical. However, the aminopyrazole compounds (**4a–4z** and **9a–9x**) reported here represent an excellent start for chemistry optimization of selective *TbGSK3* short inhibitors and an outstanding probe for studying the physiological functions of *TbGSK3* short in *T. brucei* parasites.

EXPERIMENTAL SECTION

Molecular Modeling. *Homology Modeling.* Sequence alignments between *T. brucei* and *HsGSK3β* were generated using ClustalW.²⁶ Subsequently, Modeler 9.2²⁷ was used to build homology models of *TbGSK3* short, whereas the *HsGSK3β* crystal structure (PDB code 1r0e) served as template. Modeler was run with default settings, and only the highest-scoring structure was used for further analysis and modeling.

Ligand Docking. FlexX 2.0.1 (BioSolveIT GmbH) was used to dock ligands flexible into protein binding sites.²⁸ The active sites were defined as the areas within 7 Å of the co-crystallized ligands of *HsCDK2* (PDB code 2vu3)¹⁹ and *HsGSK3β* (PDB code 1r0e)²⁹ or the equivalent residues in the homology model of *TbGSK3*. In all three structures, protonation states of amino acids and the orientations of the protons of hydroxyl and amine groups of active-site residues were manually assigned using the FlexX GUI. A highly conserved water molecule (H₂O 82 in 1r0e or H₂O 2134 in 2vu3) was kept in all three protein structures used for docking. Docking was carried out using default settings, and only the highest scoring binding modes were visually analyzed.

All figures of protein binding sites were prepared using PyMol.³⁰

Potency Screen Assays. For compound potency determinations, a radiometric 96-well Flashplate assay (PerkinElmer) was adopted. Compounds were solubilized in DMSO at a top concentration of 3 mM and serially diluted to achieve 10-point titration of final assay concentrations from $30\ \mu M$ to 0.3 nM with a final DMSO concentration of 1% (v/v). The reaction mixtures contained 1 μM biotinylated GSP2 substrate, 1 μM ATP, 3.7 KBq/well [γ -33P]-ATP and 2.5 nM *TbGSK3* in the *TbGSK3* kinase assay buffer. GSK3 inhibitors were screened for selectivity assessment also against *HsGSK3β*. For *HsGSK3* assay, the reaction mixes contained 1 μM biotinylated GSP2 substrate, 2 μM ATP, 7.4 KBq/well [γ -33P]-ATP and 15 nM *HsGSK3β* in the *TbGSK3* kinase assay buffer (25 mM Tris-HCl, pH 7.5, 10 mM MgCl₂, 5 mM DTT, 0.02% CHAPS, 2 U/mL heparin). For *HsCDK2/cyclin A* assay, the reaction mixtures contained 1 mM CDK5 biotinylated peptide substrate (Biotin-C₆-PKTPKKAKKL), 1 μM ATP, 7.4 KBq/well [γ -33P]-ATP and 2 nM *HsCDK2/cyclin A* in the kinase assay buffer (50 mM Tris-HCl, pH 7.5, 10 mM MgCl₂, 2 mM DTT, 100 mM NaCl, 0.2 mM EGTA, 0.02% (v/v) Brij35).

Statistical Evaluation of Assay Reproducibility. The statistical significance of the compound potency (IC_{50}) was based on the performance of standard molecules which have been tested to a high replication. In the case of *TbGSK3* short assay, the standard compound GW8510 was tested 93 times across 9 independent runs. The average pIC_{50} value was 8.26 with a SD (standard deviation) of 0.23. The minimum significant ratio (MSR) of 0.4 was evaluated considering the following formula:

$$\text{MSR} = 2.3 \times \text{SD}/\sqrt{N}$$

where SD is the standard deviation and N the number of replicate values routinely used for the assay (2 in our case).³¹ This implies that a difference of >0.4 in pIC_{50} can be considered statistically significant for this assay.

In the case of *HsGSK3* assay, the standard compound GW8510 was tested 47 times across 5 independent runs, with an average pIC_{50} value of 8.10 and a SD of 0.21. This implies that a difference of >0.3 in pIC_{50} can be considered statistically significant for this assay.

For the *HsCDK2* assay, the analysis was performed using two different standards (GW8510 and staurosporine) tested respectively five times in a single run and 19 times in 2 independent runs. This implies that a difference of >0.3 in pIC_{50} can be considered statistically significant for this assay.

Mammalian Kinase Profiling. Selected compounds were screened against a panel of mammalian kinases routinely run by the Division of Signal Transduction Therapy (DSTT) at the University of Dundee in duplicate at 10 μM .³² Enzymes included in the panel and assay conditions are reported in the literature. All biochemical assays are run below the K_m^{app} for the ATP for each enzyme, allowing comparison of inhibition across the panel.

Trypanosome and MRC5 Proliferation Assay. Measurement of inhibition of the proliferation of MRC5 (human lung fibroblast) cells and *T. b. brucei* bloodstream stage cells was performed using a modification of the cell viability assay previously described.³³ Compounds (50 μM to 0.5 nM) were incubated with 2×10^3 cells/well in 0.2 mL of the appropriate culture medium (MEM with 10% fetal bovine serum for MRC5 cells) in clear 96-well plates. Plates were incubated at 37 °C in the presence of 5% CO₂ for 69 h. Resazurin was then added to a final concentration of 50 μM , and plates were incubated as above for a further 4 h before being read on a BioTek flx800 fluorescent plate reader.

Chemistry. General Experimental Details. ¹H and ¹³C NMR spectra were recorded on either a Bruker Avance DPX 300 or 500 MHz spectrometer. Chemical shifts (δ) are expressed in parts per million (ppm) and coupling constants (J) are in hertz (Hz). Signal splitting patterns are described as singlet (s), broad singlet (br s), doublet (d), triplet (t), quartet (q), quintuplet (quin), sextuplet (sex), septet (sept), multiplet (m), or combinations thereof. LCMS (liquid chromatography mass spectrometry) analyses were performed with either an Agilent HPLC 1100 series connected to a Bruker Daltonics MicrOTOF or an Agilent Technologies 1200 series HPLC connected to an Agilent Technologies 6130 quadrupole LCMS, and both instruments were connected to an Agilent diode array detector. LCMS chromatographic separations were conducted with a Phenomenex Gemini C18 column, 50 mm × 3.0 mm, 5 μm particle size; mobile phase/acetonitrile +0.1% HCOOH 80:20 to 5:95 over 3.5 min, and then held for 1.5 min; flow rate 0.5 mL min⁻¹. High resolution electrospray measurements (HRMS) were performed with a Bruker Daltonics MicrOTOF mass spectrometer. Thin layer chromatography (TLC) was carried out on Merck silica gel 60 F254 plates using UV light and/or KMnO₄ for visualization. Column chromatography was performed using RediSep 4 or 12 g silica prepak columns. When applicable, all glassware was oven-dried overnight and all reactions were carried out under dry and inert conditions (Argon atmosphere).

All in this work synthesized compounds had a measured purity of greater than 95% (measured on analytical HPLC-MS system). M⁺ data are given below to substantiate the purity and integrity of the compounds. ¹H NMR, ¹³C NMR, and HRMS experiments were also used to confirm compound identity and purity.

N-((1*r*,4*r*)-4-Methoxycyclohexyl)-4-nitro-1*H*-pyrazole-3-carboxamide (2). A mixture of 4-nitro-3-pyrazolecarboxylic acid (1) (2.33 g, 14.8 mmol), *trans*-4-methoxy-cyclohexylamine (2.39 g, 18.5 mmol), EDC (3.55 g, 18.5 mmol), and HOEt (2.50 g, 18.5 mmol) in DMF (75 mL) was stirred at ambient temperature for 16 h. The mixture was reduced in vacuo and partitioned between saturated aqueous sodium bicarbonate and EtOAc. The organic layer was washed (water, brine), dried (MgSO₄), and reduced in vacuo to give a yellow oil, which was purified by column chromatography, eluting 0–100% EtOAc in petroleum ether to give 2. Yield: 3.12 g (solid), 62%. ¹H NMR (DMSO-*d*₆) δ (ppm) 14.02 (s, 1H), 8.73 (s, 1H), 8.57 (d, J = 7.81 Hz, 1H), 3.74 (m, 1H), 3.24 (s, 3H), 3.11 (m, 1H), 1.95 (dd, J = 55.8, 10.9 Hz, 4H), 1.27 (m, 4H). ¹³C NMR (DMSO-*d*₆) δ (ppm) 159.04, 141.49, 132.17, 131.44, 77.40, 55.01, 47.58, 29.67, 29.30. LRMS (ES⁺): *m/z* 269 [M + H]⁺.

4-Amino-N-(4-methoxycyclohexyl)-1*H*-pyrazole-3-carboxamide (3). A solution of 2 (1.13 g, 4.2 mmol) in DMF (100 mL) was treated with 10% palladium on carbon then shaken under hydrogen at room temperature and atmospheric pressure for 5 h. The reaction mixture was diluted with EtOAc, filtered through Celite, washing with further EtOAc, and the filtrate reduced in vacuo to give crude 3 as brown oil. Yield: 982 mg, 98%. ¹H NMR (CD₃OD) δ (ppm) 7.23 (s, 1H), 3.84 (m, 1H), 3.37 (s, 3H), 3.23 (m, 1H), 2.07 (dd, J = 45.8, 11.2 Hz, 4H), 1.38 (m, 4H). ¹³C NMR (MeOD-*d*₄) δ (ppm) 165.58, 134.15, 133.13, 118.22, 79.72, 56.15, 48.58, 31.37. LRMS (ES⁺): *m/z* 239 [M + H]⁺.

General Method for Variation of Substituent R': Example 4-Benzamido-N-(4-methoxycyclohexyl)-1*H*-pyrazole-3-carboxamide (4f). A mixture of benzoic acid (0.051 g, 0.42 mmol), 3 (0.1 g, 0.42 mmol), EDC (0.096 g, 0.5 mmol), and HOEt (0.068 g, 0.5 mmol) in DMF (10 mL) was stirred at ambient temperature for 16 h. The mixture was reduced in vacuo and partitioned between saturated aqueous sodium bicarbonate and EtOAc. The organic layer was washed (water, brine), dried (MgSO₄), and reduced in vacuo to give a creamy solid 4f, which was purified by column chromatography. Evaporation of the appropriate fraction yielded the desired compound as an amorphous solid. Yield: 39 mg, 27%. ¹H NMR (CDCl₃) δ (ppm) 10.65 (s, 1H), 8.52 (s, 1H), 8.01 (d, J = 7.2 Hz, 2H), 7.57 (t, J = 7.2 Hz, 1H), 7.51 (m, 2H), 6.86 (d, J = 8.3 Hz, 1H), 4.01 (m, 1H), 3.39 (s, 3H), 3.22 (m, 1H), 2.16 (m, 4H), 1.42 (m, 4H). ¹³C NMR (CDCl₃) δ (ppm) 164.36, 163.21, 133.54, 133.28, 132.03, 128.83, 127.24, 123.74, 120.82, 78.13, 55.91, 47.48, 30.69, 30.11. LRMS (ES⁺): *m/z* 343 [M + H]⁺. HRMS (ES⁺): calcd for C₁₈H₂₃N₄O₃ [M + H]⁺ 343.1765, found 343.1751.

4-(4,4-Difluorocyclohexanecarboxamido)-N-(4-methoxycyclohexyl)-1*H*-pyrazole-3-carboxamide (4a). Yield: 90 mg (solid) 56%. ¹H NMR (CDCl₃) δ (ppm) 9.86 (s, 1H), 8.35 (s, 1H), 6.83 (d, J = 8.3 Hz, 1H), 3.95 (m, 1H), 3.39 (s, 3H), 3.21 (m, 1H), 2.44 (m, 1H), 2.22 (m, 2H), 2.11 (m, 6H), 1.94 (m, 2H), 1.81 (m, 2H), 1.40 (m, 4H). ¹³C NMR (CDCl₃) δ (ppm) 171.61, 163.21, 133.28, 123.22, 122.55 (t, J = 239.4 Hz), 120.71, 78.07, 55.91, 47.50, 42.74, 32.85 (t, J = 23.5 Hz), 30.35, 25.73. LRMS (ES⁺): *m/z* 385 [M + H]⁺. HRMS (ES⁺): calcd for C₁₈H₂₇F₂N₄O₃ [M + H]⁺ 385.2046, found 385.2036.

N-(4-Methoxycyclohexyl)-4-(tetrahydro-2*H*-pyran-4-carboxamido)-1*H*-pyrazole-3-carboxamide (4b). Yield: 94 mg (solid), 64%. ¹H NMR (CDCl₃) δ (ppm) 9.86 (s, 1H), 8.34 (s, 1H), 6.81 (d, J = 8.1 Hz, 1H), 4.07 (m, 2H), 3.95 (m, 1H), 3.47 (m, 2H), 3.39 (s, 3H), 3.20 (m, 1H), 2.59 (m, 1H), 2.13 (d, J = 11.0 Hz, 4H), 1.91 (m, 4H), 1.40 (m, 4H). ¹³C NMR (CDCl₃) δ (ppm) 171.97, 163.30, 133.22, 123.23, 120.71, 78.12, 67.26, 55.92, 47.50, 42.20, 30.64, 30.12, 29.10. LRMS (ES⁺): *m/z* 351 [M + H]⁺. HRMS (ES⁺): calcd for C₁₇H₂₇N₄O₄ [M + H]⁺ 351.2027, found 351.2011.

4-(2-(2-Fluorophenyl)acetamido)-N-(4-methoxycyclohexyl)-1*H*-pyrazole-3-carboxamide (4c). Yield: 56 mg (solid), 71%. ¹H NMR (CD₃OD) δ (ppm) 8.20 (s, 1H), 7.38 (t, 7.7 Hz, 1H), 7.34–7.26 (m, 1H), 7.18–7.05 (m, 2H), 3.83 (m, 1H), 3.80 (s, 2H), 3.33 (s, 3H), 3.16 (m, 1H), 2.06 (br d, J = 11.5 Hz, 2H), 1.97 (br d, J = 12.0 Hz, 2H), 1.34 (m, 4H). ¹³C NMR (CD₃OD) δ (ppm) 169.57, 164.14 (d, J = 159.5 Hz), 134.23, 132.98, 130.64 (d, J = 10.9 Hz), 125.75, 123.77, 123.20 (d, J = 18.2 Hz), 121.96, 116.48 (d, J = 21.7 Hz), 79.69, 56.14, 48.68, 37.61, 31.41, 31.27. LRMS (ES⁺): *m/z* 375 [M + H]⁺. HRMS (ES⁺): calcd for C₁₉H₂₄FN₄O₃ [M + H]⁺ 375.1817, found 375.1817.

N-(4-Methoxycyclohexyl)-4-(2-(2-methoxyphenyl)acetamido)-1*H*-pyrazole-3-carboxamide (4d). Yield: 43 mg (solid), 53%. ¹H NMR (DMSO-*d*₆) δ (ppm) 13.13 (s, 1H), 9.76 (s, 1H), 8.15 (s, 1H), 8.00 (d, J = 8.3 Hz, 1H), 7.31–7.23 (m, 2H), 7.02 (d, J = 8.0 Hz, 1H), 6.93 (t, J = 7.4 Hz, 1H), 3.82 (s, 3H), 3.79–3.70 (m, 1H), 3.24 (s, 3H), 3.07 (m, 1H), 2.01 (d, J = 11.4 Hz, 2H), 1.79 (d, J = 11.4 Hz, 2H), 1.45 (m, 2H), 1.21 (m, 2H). ¹³C NMR (DMSO-*d*₆) δ (ppm) 167.30, 162.43, 157.02, 132.38, 130.90, 128.59, 123.21, 122.30, 120.44, 119.70, 110.88, 77.70, 55.41, 55.04, 46.70, 38.17, 30.26, 29.73. LRMS (ES⁺): *m/z* 387 [M + H]⁺. HRMS (ES⁺): calcd for C₂₀H₂₇N₄O₄ [M + H]⁺ 387.2027, found 387.2028.

4-(2-(2,6-Dichlorophenyl)acetamido)-N-(4-methoxycyclohexyl)-1*H*-pyrazole-3-carboxamide (4e). Yield: 63 mg (solid), 81%. ¹H NMR (DMSO-*d*₆) δ (ppm) 13.18 (br s, 1H), 9.86 (s, 1H), 8.14 (s,

1H), 8.05 (d, $J = 7.9$ Hz, 1H), 7.51 (d, $J = 8.2$ Hz, 2H), 7.36 (t, $J = 8.2$ Hz, 1H), 4.10 (s, 2H), 3.76 (m, 1H), 3.24 (s, 3H), 3.08 (s, 1H), 2.01 (m, 2H), 1.81 (m, 2H), 1.45 (m, 2H), 1.19 (m, 2H). ^{13}C NMR (DMSO- d_6) δ (ppm) 170.16, 162.31, 135.49, 131.62, 129.68, 128.30, 128.10, 122.23, 122.09, 77.68, 55.04, 46.77, 38.23, 30.25, 29.74. LRMS (ES $^+$): m/z 425 [M + H] $^+$. HRMS (ES $^+$): calcd for $\text{C}_{19}\text{H}_{23}\text{Cl}_2\text{N}_4\text{O}_3$ [M + H] $^+$ 425.1142, found 425.1147.

4-(2-Fluorobenzamido)-N-(4-methoxycyclohexyl)-1H-pyrazole-3-carboxamide (4g**).** Yield: 97 mg (solid), 64%. ^1H NMR (CDCl_3) δ (ppm) 10.89 (d, $J = 12.2$ Hz, 1H), 8.45 (s, 1H), 8.07 (m, 1H), 7.44 (m, 1H), 7.22 (m, 1H), 7.13 (m, 1H), 6.73 (d, $J = 8.3$ Hz, 1H), 3.96 (m, 1H), 3.29 (s, 3H), 3.11 (m, 1H), 2.05 (m, 4H), 1.31 (m, 4H). ^{13}C NMR (CDCl_3) δ (ppm) 162.80, 160.84 (d, $J = 246.9$ Hz), 160.53, 133.81 (d, $J = 10.9$ Hz), 131.77, 124.79, 123.19, 121.42, 120.65 (d, $J = 10.7$ Hz), 116.46 (d, $J = 21.8$ Hz), 78.19, 55.88, 47.27, 30.75, 30.14. LRMS (ES $^+$): m/z 361 [M + H] $^+$. HRMS (ES $^+$): calcd for $\text{C}_{18}\text{H}_{22}\text{FN}_4\text{O}_3$ [M + H] $^+$ 361.1670, found 361.1645.

N-(4-Methoxycyclohexyl)-4-(2-(trifluoromethyl)benzamido)-1H-pyrazole-3-carboxamide (4h**).** Yield: 67 mg (solid), 78%. ^1H NMR (DMSO- d_6) δ (ppm) 13.40 (s, 1H), 10.22 (s, 1H), 8.32 (s, 1H), 8.29 (d, $J = 8.6$ Hz, 1H), 7.90–7.88 (m, 1H), 7.84–7.81 (m, 1H), 7.78–7.75 (m, 2H), 3.72 (m, 1H), 3.23 (s, 3H), 3.06 (m, 1H), 2.00 (br d, $J = 12.5$ Hz, 2H), 1.76 (br d, $J = 12.5$ Hz, 2H), 1.45 (m, 2H), 1.14 (m, 2H). ^{13}C NMR (DMSO- d_6) δ (ppm) 163.34, 162.73, 135.06, 133.01, 132.78, 130.73, 128.39, 126.63 (d, $J = 5.2$ Hz) 126.04 (d, $J = 29.1$ Hz), 123.57 (d, $J = 276.3$ Hz), 122.06, 120.30, 77.66, 55.06, 46.97, 30.28, 29.67. LRMS (ES $^+$): m/z 411 [M + H] $^+$. HRMS (ES $^+$): calcd for $\text{C}_{19}\text{H}_{22}\text{F}_3\text{N}_4\text{O}_3$ [M + H] $^+$ 411.1639, found 411.1621.

4-(2-Ethylbenzamido)-N-(4-methoxycyclohexyl)-1H-pyrazole-3-carboxamide (4i**).** Yield: 63 mg (solid), 81%. ^1H NMR (CDCl_3) δ (ppm) 10.04 (s, 1H), 8.39 (s, 1H), 7.53 (d, $J = 7.6$ Hz, 1H), 7.39 (t, $J = 7.6$ Hz, 1H), 7.30 (d, $J = 7.7$ Hz, 1H), 7.25 (t, $J = 7.5$ Hz, 1H), 6.87 (d, $J = 8.3$ Hz, 1H), 3.92 (m, 1H), 3.36 (s, 3H), 3.16 (m, 1H), 2.90 (q, $J = 7.6$ Hz, 2H), 2.08 (br d, $J = 10.0$ Hz, 4H), 1.35 (m, 4H), 1.26 (t, $J = 7.6$ Hz, 3H). ^{13}C NMR (CDCl_3) δ (ppm) 167.60, 163.29, 142.86, 134.89, 133.19, 130.65, 129.69, 127.15, 126.11, 123.25, 120.94, 78.18, 55.86, 74.45, 30.58, 30.12, 26.44, 15.84. LRMS (ES $^+$): m/z 371 [M + H] $^+$. HRMS (ES $^+$): calcd for $\text{C}_{20}\text{H}_{27}\text{N}_4\text{O}_3$ [M + H] $^+$ 371.2078, found 371.2078.

4-(2-Methoxybenzamido)-N-(4-methoxycyclohexyl)-1H-pyrazole-3-carboxamide (4j**).** Yield: 35 mg (solid), 45%. ^1H NMR (DMSO- d_6) δ (ppm) 13.25 (s, 1H), 11.77 (s, 1H), 8.44 (s, 1H), 8.15 (s, 1H), 8.04 (s, 1H), 7.63 (s, 1H), 7.29 (s, 1H), 7.18 (s, 1H), 4.15 (s, 3H), 3.88 (m, 1H), 3.30 (s, 3H), 3.16 (m, 1H), 2.08 (m, 2H), 1.91 (m, 2H), 1.55 (m, 2H), 1.29 (m, 2H). ^{13}C NMR (DMSO- d_6) δ (ppm) 162.43, 160.94, 157.47, 133.49, 131.33, 122.29, 120.83, 120.59, 120.28, 112.32, 77.73, 56.05, 55.05, 46.72, 30.28, 29.83. LRMS (ES $^+$): m/z 373 [M + H] $^+$. HRMS (ES $^+$): calcd for $\text{C}_{19}\text{H}_{25}\text{N}_4\text{O}_4$ [M + H] $^+$ 373.1870, found 373.1873.

N-(4-Methoxycyclohexyl)-4-(2-(phenylamino)benzamido)-1H-pyrazole-3-carboxamide (4k**).** Yield: 41 mg (solid), 45%. ^1H NMR (DMSO- d_6) δ (ppm) 13.32 (br s, 1H), 10.93 (s, 1H), 9.53 (s, 1H), 8.31 (s, 1H), 8.28 (d, $J = 8.5$ Hz, 1H), 7.68 (dd, $J = 8.0, 1.4$ Hz, 1H), 7.43 (m, 1H), 7.33–7.28 (m, 3H), 7.16–7.14 (m, 2H), 7.01–6.96 (m, 2H), 3.82 (m, 1H), 3.35 (s, 1H), 3.25 (s, 3H), 3.09 (m, 1H), 2.03 (br d, $J = 12.0$ Hz, 2H), 1.81 (br d, $J = 12.0$ Hz, 2H), 1.48 (m, 2H), 1.20 (m, 2H). ^{13}C NMR (DMSO- d_6) δ (ppm) 164.84, 162.97, 144.57, 141.62, 132.81, 129.33, 128.04, 122.32, 122.00, 120.01, 119.63, 119.26, 118.30, 116.49, 77.74, 55.06, 46.95, 30.33, 29.73. LRMS (ES $^+$): m/z 434 [M + H] $^+$. HRMS (ES $^+$): calcd for $\text{C}_{24}\text{H}_{28}\text{N}_5\text{O}_3$ [M + H] $^+$ 434.2187, found 434.2165.

4-(2-((2,3-Dimethylphenyl)amino)benzamido)-N-(4-methoxycyclohexyl)-1H-pyrazole-3-carboxamide (4l**).** Yield: 53 mg (solid), 55%. ^1H NMR (DMSO- d_6) δ (ppm) 13.35 (br s, 1H), 10.89 (s, 1H), 9.53 (s, 1H), 8.33 (s, 1H), 7.63 (dd, $J = 8.1, 1.4$ Hz, 1H), 7.34 (m, 1H), 7.11–7.09 (m, 2H), 6.99–6.97 (m, 1H), 6.87 (m, 1H), 6.82 (dd, $J = 8.4, 1.0$ Hz, 1H), 3.84 (m, 1H), 3.35 (s, 1H), 3.25 (s, 3H), 3.09 (m, 1H), 2.29 (s, 3H), 2.14 (s, 3H), 2.03 (br d, $J = 12.0$ Hz, 2H), 1.82 (br d, $J = 12.0$ Hz, 2H), 1.49 (m, 2H), 1.21 (m, 2H). ^{13}C NMR (DMSO- d_6) δ (ppm) 165.36, 163.08, 147.05, 138.87, 137.74, 132.95, 132.72,

130.25, 127.52, 125.96, 125.74, 122.41, 120.79, 119.98, 117.44, 115.36, 114.63, 77.74, 55.06, 46.95, 30.33, 29.75, 20.25, 13.64. LRMS (ES $^+$): m/z 462 [M + H] $^+$. HRMS (ES $^+$): calcd for $\text{C}_{26}\text{H}_{32}\text{N}_5\text{O}_3$ [M + H] $^+$ 462.2500, found 462.2503.

4-(2,6-Dimethoxybenzamido)-N-(4-methoxycyclohexyl)-1H-pyrazole-3-carboxamide (4m**).** Yield: 73 mg, 43% (solid). ^1H NMR (DMSO- d_6) δ (ppm) 13.28 (s, 1H), 9.75 (s, 1H), 8.29 (s, 1H), 8.20 (d, $J = 8.4$ Hz, 1H), 7.39 (t, $J = 8.5$ Hz, 1H), 6.75 (d, $J = 8.5$ Hz, 2H), 3.76 (s, 6H), 3.70 (m, 1H), 3.22 (s, 3H), 3.06 (m, 1H), 2.00 (m, 2H), 1.76 (m, 2H), 1.45 (m, 2H), 1.13 (m, 2H). ^{13}C NMR (DMSO- d_6) δ (ppm) 162.79, 161.21, 156.88, 132.21, 131.08, 122.52, 119.81, 115.03, 104.28, 77.66, 55.81, 55.08, 46.93, 30.29, 29.66. LRMS (ES $^+$): m/z 403 [M + H] $^+$. HRMS (ES $^+$): calcd for $\text{C}_{20}\text{H}_{27}\text{N}_4\text{O}_5$ [M + H] $^+$ 403.1976, found 403.1960.

N-(4-Methoxycyclohexyl)-4-(2,4,6-trimethoxybenzamido)-1H-pyrazole-3-carboxamide (4n**).** Yield: 76 mg (solid), 84%. ^1H NMR (CD_3OD) δ (ppm) 8.36 (s, 1H), 6.17 (s, 2H), 3.84 (s, 3H), 3.82 (s, 6H), 3.35 (s, 3H), 3.22 (m, 1H), 2.08 (m, 4H), 1.36 (m, 4H). ^{13}C NMR (CD_3OD) δ (ppm) 164.90, 164.72, 164.35, 160.74, 134.07, 124.36, 122.58, 108.39, 92.09, 79.74, 57.05, 56.89, 56.62, 48.71, 31.61, 31.40. LRMS (ES $^+$): m/z 433 [M + H] $^+$. HRMS (ES $^+$): calcd for $\text{C}_{21}\text{H}_{29}\text{N}_4\text{O}_6$ [M + H] $^+$ 433.2082, found 433.2065.

4-(2,4-Difluorobenzamido)-N-(4-methoxycyclohexyl)-1H-pyrazole-3-carboxamide (4o**).** Yield: 114 mg (solid), 72%. ^1H NMR (DMSO- d_6) δ (ppm) 13.24 (s, 1H), 10.89 (d, $J = 10.2$ Hz, 1H), 8.33 (s, 1H), 8.09 (q, $J = 8.7$ Hz, 1H), 8.05 (d, $J = 8.4$ Hz, 1H), 7.39 (m, 1H), 7.24 (m, 1H), 3.82 (m, 1H), 3.25 (s, 3H), 3.10 (m, 1H), 2.02 (d, $J = 10.3$ Hz, 2H), 1.84 (d, $J = 11.6$ Hz, 2H), 1.47 (q, $J = 12.0$ Hz, 2H), 1.22 (q, $J = 12.5$ Hz, 2H). ^{13}C NMR (DMSO- d_6) δ (ppm) 164.3 (q, $J = 250.6, 10.9$ Hz), 162.71, 160.3 (q, $J = 250.8, 14.5$ Hz), 158.03, 133.26, 133.18, 132.82, 122.12, 120.50, 117.39, 117.31, 112.59, 112.42, 104.96, 104.75, 104.52, 79.12, 78.84, 78.58, 77.71, 55.07, 46.89, 30.09, 29.76. LRMS (ES $^+$): m/z 379 [M + H] $^+$. HRMS (ES $^+$): calcd for $\text{C}_{18}\text{H}_{21}\text{F}_2\text{N}_4\text{O}_3$ [M + H] $^+$ 379.1576, found 379.1567.

4-(3,5-Difluorobenzamido)-N-(4-methoxycyclohexyl)-1H-pyrazole-3-carboxamide (4p**).** Yield: 157 mg (solid), 99%. ^1H NMR (DMSO- d_6) δ (ppm) 13.39 (s, 1H), 10.77 (s, 1H), 8.34 (d, $J = 8.5$ Hz, 1H), 8.30 (s, 1H), 7.59 (m, 1H), 7.52 (m, 2H), 3.84 (m, 1H), 3.24 (s, 3H), 3.09 (m, 1H), 2.02 (d, $J = 10.7$ Hz, 2H), 1.81 (d, $J = 10.7$ Hz, 2H), 1.49 (q, $J = 11.8$ Hz, 2H), 1.20 (q, $J = 11.8$ Hz, 2H). ^{13}C NMR (DMSO- d_6) δ (ppm) 162.8, 162.5 (q, $J = 250.7, 14.4$ Hz), 160.3, 137.16, 127.75, 126.59, 124.12, 122.13, 118.94, 110.2 (q, $J = 22.0, 14.5$ Hz), 107.5 (t, $J = 27.0$ Hz), 77.71, 55.06, 46.99, 30.29, 29.76. LRMS (ES $^+$): m/z 379 [M + H] $^+$. HRMS (ES $^+$): calcd for $\text{C}_{18}\text{H}_{21}\text{F}_2\text{N}_4\text{O}_3$ [M + H] $^+$ 379.1568.

4-(3,5-Dichlorobenzamido)-N-(4-methoxycyclohexyl)-1H-pyrazole-3-carboxamide (4q**).** Yield: 147 mg (solid), 85%. ^1H NMR (CDCl_3) δ (ppm) 10.34 (s, 1H), 8.23 (s, 1H), 7.60 (d, $J = 1.9$ Hz, 2H), 7.31 (t, $J = 1.8$ Hz, 1H), 7.05 (s, 1H), 6.58 (d, 1H), 3.77 (m, 1H), 3.15 (s, 3H), 2.98 (m, 1H), 1.91 (m, 4H), 1.18 (m, 4H). ^{13}C NMR (DMSO- d_6) δ (ppm) 163.12, 161.74, 136.46, 135.73, 131.89, 128.34, 126.03, 125.79, 121.09, 78.10, 55.91, 47.48, 30.69, 30.08. LRMS (ES $^+$): m/z 411 [M + H] $^+$. HRMS (ES $^+$): calcd for $\text{C}_{18}\text{H}_{21}\text{Cl}_2\text{N}_4\text{O}_3$ [M + H] $^+$ 411.0985, found 411.0966.

4-(4-Difluoromethoxy)benzamido-N-(4-methoxycyclohexyl)-1H-pyrazole-3-carboxamide (4r**).** Yield: 96 mg (solid), 56%. ^1H NMR (CDCl_3) δ (ppm) 10.65 (s, 1H), 8.48 (s, 1H), 8.02 (d, $J = 8.6$ Hz, 2H), 7.24 (d, $J = 8.6$ Hz, 2H), 6.84 (d, $J = 8.3$ Hz, 1H), 6.62 (t, $J = 73.2$ Hz, 1H), 4.00 (m, 1H), 3.39 (s, 3H), 3.22 (m, 1H), 2.15 (m, 4H), 1.42 (m, 4H). ^{13}C NMR (CDCl_3) δ (ppm) 163.28, 163.20, 154.0 (t, $J = 2.9$ Hz), 133.56, 130.28, 129.24, 123.64, 120.74, 119.22, 118.94, 115.47, 112.01, 78.11, 55.94, 47.53, 30.67, 30.12. LRMS (ES $^+$): m/z 409 [M + H] $^+$. HRMS (ES $^+$): calcd for $\text{C}_{19}\text{H}_{23}\text{F}_2\text{N}_4\text{O}_4$ [M + H] $^+$ 409.1682, found 409.1649.

N-(4-Methoxycyclohexyl)-4-(4-(pyrrolidin-1-yl)benzamido)-1H-pyrazole-3-carboxamide (4s**).** Yield: 73 mg (solid), 42%. ^1H NMR (CDCl_3) δ (ppm) 10.44 (s, 1H), 8.49 (s, 1H), 7.89 (d, $J = 8.8$ Hz, 2H), 6.85 (d, $J = 8.3$ Hz, 1H), 6.62 (d, $J = 8.8$ Hz, 2H), 4.01 (m, 1H), 3.39 (m, 7H), 3.20 (m, 1H), 2.15 (m, 4H), 2.06 (m, 4H), 1.41 (m, 4H). ^{13}C NMR (CDCl_3) δ (ppm) 164.74, 163.48, 150.26, 133.26,

128.99, 124.26, 120.52, 119.42, 111.20, 78.20, 55.92, 47.66, 47.39, 30.73, 30.18, 25.46. LRMS (ES⁺): *m/z* 412 [M + H]⁺. HRMS (ES⁺): calcd for C₂₂H₃₀N₆O₃ [M + H]⁺ 412.2343, found 412.2338.

N-(4-Methoxycyclohexyl)-4-(4-methylpipеразин-1-yl)-benzamido-1H-pyrazole-3-carboxamide (4t). Yield: 37 mg (solid), 20%. ¹H NMR (CDCl₃) δ (ppm) 10.48 (s, 1H), 8.47 (s, 1H), 7.90 (d, *J* = 8.8 Hz, 2H), 6.94 (d, *J* = 8.8 Hz, 2H), 6.83 (m, 1H), 4.00 (m, 1H), 3.39 (s, 3H), 3.37 (t, *J* = 5 Hz, 4H), 3.20 (m, 1H), 2.60 (t, *J* = 5 Hz, 4H), 2.38 (s, 3H), 2.14 (m, 4H), 1.41 (m, 4H). ¹³C NMR (CDCl₃) δ (ppm) 164.17, 163.44, 153.54, 133.33, 128.81, 124.05, 122.92, 120.61, 114.27, 78.17, 55.92, 54.79, 47.62, 47.41, 46.11, 30.72, 30.17. LRMS (ES⁺): *m/z* 441 [M + H]⁺. HRMS (ES⁺): calcd for C₂₃H₃₃N₆O₃ [M + H]⁺ 441.2609, found 441.2597.

4-Benzofuran-2-carboxamido-N-(4-methoxycyclohexyl)-1H-pyrazole-3-carboxamide (4u). Yield: 134 mg (solid), 83%. ¹H NMR (CDCl₃) δ (ppm) 10.76 (s, 1H), 8.53 (s, 1H), 7.70 (d, *J* = 7.5 Hz, 1H), 7.66 (d, *J* = 8.4 Hz, 1H), 7.59 (d, *J* = 0.9 Hz, 1H), 7.46 (t, *J* = 7.8 Hz, 1H), 7.33 (t, *J* = 7.5 Hz, 1H), 6.85 (d, *J* = 8.4 Hz, 1H), 4.07 (m, 1H), 3.40 (s, 3H), 3.22 (m, 1H), 2.16 (m, 4H), 1.43 (m, 4H). ¹³C NMR (CDCl₃) δ (ppm) 163.03, 156.21, 155.22, 148.18, 133.76, 129.23, 127.56, 127.24, 123.77, 122.59, 121.20, 112.41, 111.23, 78.15, 55.91, 47.41, 30.74, 30.14. LRMS (ES⁺): *m/z* 383 [M + H]⁺. HRMS (ES⁺): calcd for C₂₀H₂₃N₄O₄ [M + H]⁺ 383.1714, found 383.1703.

N-(3-((4-Methoxycyclohexyl)carbamoyl)-1H-pyrazol-4-yl)-pyrazolo[1,5-a]pyridine-2-carboxamide (4v). Yield: 115 mg (solid), 72%. ¹H NMR (DMSO-d₆) δ (ppm) 13.30 (s, 1H), 11.01 (s, 1H), 8.83 (d, *J* = 7.0 Hz, 1H), 8.37 (s, 1H), 8.15 (d, *J* = 8.4 Hz, 1H), 7.82 (d, *J* = 8.9 Hz, 1H), 7.34 (t, *J* = 7.7 Hz, 1H), 7.09 (t, *J* = 6.9 Hz, 1H), 3.85 (m, 1H), 3.26 (s, 3H), 3.11 (m, 1H), 2.04 (d, *J* = 10.3 Hz, 2H), 1.84 (d, *J* = 10.7 Hz, 2H), 1.49 (m, 2H), 1.23 (m, 2H). ¹³C NMR (DMSO-d₆) δ (ppm) 162.70, 158.15, 146.85, 141.15, 132.80, 128.99, 124.60, 122.00, 120.08, 119.14, 114.53, 97.79, 77.74, 55.06, 46.95, 30.33, 29.79. LRMS (ES⁺): *m/z* 383 [M + H]⁺. HRMS (ES⁺): calcd for C₁₉H₂₃N₆O₃ [M + H]⁺ 383.1826, found 383.1812.

N-(3-((4-Methoxycyclohexyl)carbamoyl)-1H-pyrazol-4-yl)-imidazo[1,2-a]pyridine-3-carboxamide (4w). Yield: 11 mg (solid), 7%. ¹H NMR (MeOD-d₄) δ (ppm) 9.57 (d, *J* = 6.9 Hz, 1H), 8.31 (d, *J* = 8.3 Hz, 2H), 7.74 (d, *J* = 9.0 Hz, 1H), 7.57 (td, *J* = 6.9, 1.2 Hz, 1H), 7.19 (t, *J* = 6.9, 1.2 Hz, 1H), 3.94 (m, 1H), 3.39 (s, 3H), 3.27 (m, 1H), 2.12 (m, 4H), 1.50 (m, 2H), 1.39 (m, 2H). ¹³C NMR (DMSO-d₆) δ (ppm) 162.89, 156.52, 147.37, 136.35, 127.61, 127.41, 122.12, 119.89, 117.57, 117.46, 114.43, 77.71, 55.07, 46.90, 30.30, 29.76. LRMS (ES⁺): *m/z* 383 [M + H]⁺. HRMS (ES⁺): calcd for C₁₉H₂₃N₆O₃ [M + H]⁺ 383.1826, found 383.1811.

N-(3-((4-Methoxycyclohexyl)carbamoyl)-1H-pyrazol-4-yl)-2-methylimidazo[1,2-a]pyridine-3-carboxamide (4x). Yield: 47 mg (solid), 28%. ¹H NMR (CDCl₃) δ (ppm) 10.88 (s, 1H), 10.24 (s, 1H), 9.58 (d, *J* = 6.9 Hz, 1H), 8.51 (s, 1H), 7.67 (d, *J* = 9.0 Hz, 1H), 7.41 (t, *J* = 7.9 Hz, 1H), 6.99 (t, *J* = 6.9 Hz, 1H), 6.80 (d, *J* = 7.9 Hz, 1H), 4.01 (m, 1H), 3.39 (s, 3H), 3.21 (m, 1H), 3.02 (s, 3H), 2.14 (m, 4H), 1.41 (m, 4H). ¹³C NMR (DMSO-d₆) δ (ppm) 162.73, 157.27, 146.18, 145.49, 127.61, 127.42, 122.35, 120.04, 116.31, 114.46, 113.62, 77.74, 55.06, 46.77, 30.24, 29.81, 16.52. LRMS (ES⁺): *m/z* 397 [M + H]⁺. HRMS (ES⁺): calcd for C₂₀H₂₅N₆O₃ [M + H]⁺ 397.1983, found 397.1972.

N-(4-Methoxycyclohexyl)-4-(5-phenylfuran-2-carboxamido)-1H-pyrazole-3-carboxamide (4y). Yield: 107 mg (solid), 62%. ¹H NMR (CDCl₃): δ (ppm) 10.61 (s, 1H), 8.49 (s, 1H), 7.84 (m, 2H), 7.48 (t, *J* = 7.5 Hz, 2H), 7.38 (t, *J* = 7.4 Hz, 1H), 7.31 (t, *J* = 3.6 Hz, 1H), 6.85 (d, *J* = 8.5 Hz, 1H), 6.80 (d, *J* = 3.6 Hz, 1H), 4.07 (m, 1H), 3.40 (s, 3H), 3.22 (m, 1H), 2.16 (m, 4H), 1.42 (m, 4H). ¹³C NMR (CDCl₃) δ (ppm) 163.03, 156.39, 155.72, 146.33, 133.74, 129.49, 128.94, 128.80, 124.72, 122.85, 120.91, 117.13, 107.30, 78.18, 55.88, 47.25, 30.78, 30.14. LRMS (ES⁺): *m/z* 409 [M + H]⁺. HRMS (ES⁺): calcd for C₂₂H₂₅N₆O₄ [M + H]⁺ 409.1870, found 409.1832.

N-(3-((4-Methoxycyclohexyl)carbamoyl)-1H-pyrazol-4-yl)-5-phenyloxazole-4-carboxamide (4z). Yield: 71 mg (solid), 41%. ¹H NMR (DMSO-d₆) δ (ppm) 13.30 (s, 1H), 11.20 (s, 1H), 8.68 (s, 1H), 8.38 (s, 1H), 8.30 (m, 2H), 8.14 (d, *J* = 8.4 Hz, 1H), 7.58–7.51 (m, 3H), 3.83 (m, 1H), 3.26 (s, 3H), 3.11 (m, 1H), 2.04 (d, *J* = 10.5 Hz, 2H),

1.84 (d, *J* = 11.0 Hz, 2H), 1.49 (q, *J* = 12.5 Hz, 2H), 1.23 (q, *J* = 11.5 Hz, 2H). ¹³C NMR (DMSO-d₆) δ (ppm) 162.64, 157.34, 151.99, 150.43, 132.90, 130.23, 128.50, 128.07, 127.92, 126.62, 121.89, 120.02, 77.74, 55.06, 47.00, 30.33, 29.76. LRMS (ES⁺): *m/z* 410 [M + H]⁺. HRMS (ES⁺): calcd for C₂₁H₂₄N₆O₄ [M + H]⁺ 410.1823, found 410.1807.

Methyl 4-Nitro-1H-pyrazole-3-carboxylate (5). A 100 mL three-necked round-bottomed flask equipped with a magnetic stirring bar and fitted with a dropping funnel was charged with 4-nitro-1H-pyrazole-3-carboxylic acid (4.0 g, 25.5 mmol) and methanol (40 mL). The flask was cooled to 0 °C, and thionyl chloride (2.1 mL, 28.9 mmol) was added to the vigorously stirred solution over a period of 10 min. The mixture was stirred for an additional 12 h at room temperature, after which time TLC indicated complete consumption of the starting acid. The reaction mixture was concentrated under reduced pressure at 40 °C and the residue treated with toluene and reconcentrated (3 × 20 mL) under reduced pressure at 40 °C to give methyl ester 5 as an off-white solid. Yield: 4.42 g, 99%. ¹H NMR (DMSO-d₆) δ (ppm) 14.39 (br s, 1H), 9.98 (s, 1H), 3.90 (s, 3H). ¹³C NMR (DMSO-d₆) δ (ppm) 161.15, 138.13, 133.20, 130.90, 52.84. LRMS (ES⁺): *m/z* 172 [M + H]⁺.

Methyl-4-amino-1H-pyrazole-3-carboxylate (6). A 100 mL round-bottomed flask equipped with digital thermometer and stirrer was charged with 10% palladium on carbon (0.621 g) under argon. In a separate vessel, a slurry of methyl ester 5 (4.42 g, 25.8 mmol) in ethanol (45 mL) was warmed to 35 °C to effect dissolution and the solution added to the catalyst under argon. Following a nitrogen–hydrogen purge sequence, an atmosphere of hydrogen was introduced and the reaction mixture maintained at 30 °C until the reaction completion (6 h) was noted by ¹H NMR analysis. Following a purge cycle, the reaction mixture under argon was filtered and the liquors concentrated under reduced pressure to give amine 6 as a solid. Yield: 3.57 g, 98%. ¹H NMR (DMSO-d₆) δ (ppm) 12.83 (br s, 1H), 7.10 (s, 1H), 4.83 (br s, 2H), 3.78 (s, 3H). ¹³C NMR (DMSO-d₆) δ (ppm) 160.39, 136.94, 128.43, 115.59, 50.88. LRMS (ES⁺): *m/z* 142 [M + H]⁺.

Methyl-4-(2,6-dimethoxybenzamido)-1H-pyrazole-3-carboxylate (7). A solution of amine 6 (3.57 g, 25.3 mmol) in 1,4-dioxane (50 mL) under argon was treated with triethylamine (4.3 mL, 31 mmol) followed by 2,6-dimethoxybenzoyl chloride (6.13 g, 30.6 mmol) such that the internal temperature was maintained in the range 20–25 °C. The reaction mixture was stirred at 25 °C until the reaction was complete (12 h) by TLC analysis. The reaction mixture was filtered, the filter-cake washed with 1,4-dioxane, and the combined filtrates progressed to next stage without further isolation.

To obtain analytical data for compound 7 and also to determine the yield of this reaction, a 2 g sample was taken out of the homogeneous filtrate solution (total weight of this solution is 91g). The 2 g sample was then concentrated under reduced pressure until dryness. The crude product (~192 mg) was purified by column chromatography (DCM/MeOH). Evaporation of the appropriate fractions yielded finally the desired compound 7 as an amorphous solid (161 mg). Therefore, in the whole filtrate contained 7.33 g of compound 7. A 5 mg sample was used for to obtain analytical data; the rest was redissolved for use in the next reaction. Yield: 7.33 g, 95%. ¹H NMR (DMSO-d₆) 13.68 (br s, 1H), 9.16 (s, 1H), 8.31 (s, 1H), 7.41 (t, *J* = 8.4 Hz, 1H), 6.76 (d, *J* = 8.4 Hz, 2H), 3.83 (s, 3H), 3.77 (s, 6H). ¹³C NMR (DMSO-d₆) δ (ppm) 163.86, 161.55, 157.07, 131.27, 129.97, 123.61, 120.41, 114.66, 104.35, 55.84, 51.63. LRMS (ES⁺): *m/z* 306 [M + H]⁺. HRMS (ES⁺): calcd for C₁₄H₁₆N₃O₅ [M + H]⁺ 306.1084, found 306.1081.

4-(2,6-Dimethoxybenzamido)-1H-pyrazole-3-carboxylic Acid (8). To a solution of sodium hydroxide (3.32 g, 83 mmol) in water (20 mL) was charged a solution of ester 7 in one portion (7.33 g, 24.0 mmol; the solution of crude 7 from the previous reaction, plus 156 mg of redissolved pure 7). The reaction mixture was stirred at 25 °C until completion as determined by TLC analysis. The reaction mixture was concentrated under reduced pressure at 45 °C, the oily residue diluted with water and acidified to pH 1 with concentrated hydrochloric acid, such that the temperature was maintained below 30 °C. The resulting

precipitate was collected by filtration, washed with water, pulled dry on the filter, and subsequently washed with heptanes. The filter cake was charged to a 200 mL rotary evaporator flask and drying completed azeotropically with toluene. Yield: 6.22 g, 89%. ¹H NMR (DMSO-*d*₆) 13.44 (br s, 2H), 9.17 (br s, 1H), 8.29 (s, 1H), 7.40 (t, *J* = 8.4 Hz, 1H), 6.76 (d, *J* = 8.4 Hz, 2H), 3.77 (s, 6H). LRMS (ES⁺): *m/z* 292 [M + H]⁺. HRMS (ES⁺): calcd for C₁₃H₁₄N₃O₅ [M + H]⁺ 292.0928, found 292.0920.

General Method for Variation of Substituent R²: Example N-Cyclohexyl-4-(2,6-dimethoxybenzamido)-1H-pyrazole-3-carboxamide (9c). A mixture of carboxylic acid (50 mg, 0.17 mmol, 1.2 equiv), amine (14 mg, 0.14 mmol, 1.0 equiv), hydroxybenzotriazole (19 mg, 0.14 mmol, 1.0 equiv), polymer-supported-carbodiimide (105 mg, 0.14 mmol, 1.0 equiv), and acetonitrile was heated by microwave irradiation for 10 min at 100 °C. The final product (9c) was isolated from the reaction mixture by filtering through a short column of Si-carbonate under gravity, which scavenged the excess carboxylic acid and hydroxybenzotriazole. No further purification was required. Removal of the solvent under reduced pressure yielded the required compounds as amorphous solids. Yield: 49 mg (solid), 67%. ¹H NMR (CD₃OD) δ (ppm) 8.33 (s, 1H), 7.42 (t, *J* = 8.4 Hz, 1H), 6.75 (d, *J* = 8.4 Hz, 2H), 3.86 (s, 6H), 3.82 (m, 1H), 1.88 (m, 4H), 1.68 (d, *J* = 12.8 Hz, 1H), 1.40 (m, 4H), 1.27 (m, 1H). ¹³C NMR (CD₃OD) δ (ppm) 165.02, 164.71, 159.24, 134.17, 132.97, 123.89, 121.82, 115.64, 105.24, 56.50, 49.36, 33.77, 26.58, 26.19. LRMS (ES⁺): *m/z* 373 [M + H]⁺. HRMS (ES⁺): calcd for C₁₉H₂₅N₄O₄ [M + H]⁺ 373.1870, found 373.1850.

N-Cyclopropyl-4-(2,6-dimethoxybenzamido)-1H-pyrazole-3-carboxamide (9a). Yield: 42 mg (solid), 64%. ¹H NMR (CD₃OD) δ (ppm) 8.32 (s, 1H), 7.42 (t, *J* = 8.4 Hz, 1H), 6.76 (d, *J* = 8.4 Hz, 2H), 3.86 (s, 6H), 2.79 (m, 1H), 0.80 (m, 2H), 0.65 (m, 2H). ¹³C NMR (DMSO-*d*₆) δ (ppm) 161.32, 161.20, 131.10, 122.44, 122.30, 115.01, 104.28, 55.82, 22.13, and 22.02 (d, rotamers), 5.55. LRMS (ES⁺): *m/z* 331 [M + H]⁺. HRMS (ES⁺): calcd for C₁₆H₁₉N₄O₄ [M + H]⁺ 331.1401, found 331.1385.

N-Cyclobutyl-4-(2,6-dimethoxybenzamido)-1H-pyrazole-3-carboxamide (9b). Yield: 56 mg (solid), 94%. ¹H NMR (DMSO-*d*₆) δ (ppm) 13.28 (s, 1H), 9.71 (s, 1H), 8.60 (d, *J* = 8.1 Hz, 1H), 8.30 (s, 1H), 7.40 (t, *J* = 8.4 Hz, 1H), 6.74 (d, *J* = 8.4 Hz, 2H), 4.37 (sex, *J* = 8.3, 1H), 3.76 (s, 6H), 2.13 (m, 4H), 1.63 (m, 2H). ¹³C NMR (DMSO-*d*₆) δ (ppm) 162.53, 161.23, 156.93, 132.14, 131.07, 122.61, 119.84, 115.07, 104.32, 55.82, 54.86, 43.39, 29.81, 14.62. LRMS (ES⁺): *m/z* 345 [M + H]⁺. HRMS (ES⁺): calcd for C₁₇H₂₁N₄O₄ [M + H]⁺ 345.1557, found 345.1548.

N-Cycloheptyl-4-(2,6-dimethoxybenzamido)-1H-pyrazole-3-carboxamide (9d). Yield: 60 mg (solid), 90%. ¹H NMR (CDCl₃) δ (ppm) 12.19 (br s, 1H), 9.94 (s, 1H), 8.41 (s, 1H), 7.29 (t, *J* = 8.5 Hz, 1H), 6.98 (d, *J* = 8.1 Hz, 1H), 6.57 (d, *J* = 8.5 Hz, 2H), 4.05 (m, 1H), 3.80 (s, 6H), 2.00–1.94 (m, 2H), 1.66–1.45 (m, 10H). ¹³C NMR (CDCl₃) δ (ppm) 161.75, 160.98, 155.95, 131.18, 129.57, 121.16, 119.75, 112.84, 102.24, 54.19, 48.30, 33.28, 26.12, 22.39. LRMS (ES⁺): *m/z* 387 [M + H]⁺. HRMS (ES⁺): calcd for C₂₀H₂₇N₄O₄ [M + H]⁺ 387.2027, found 387.2043.

N-[Bicyclo[2.2.1]heptan-2-yl]-4-(2,6-dimethoxybenzamido)-1H-pyrazole-3-carboxamide (9e). Yield: 49 mg (solid), 52%. ¹H NMR (DMSO-*d*₆) δ (ppm) 11.80 (br s, 1H), 9.72 (s, 1H), 8.28 (s, 1H), 8.00 (br d, *J* = 6.9 Hz, 1H), 7.40 (t, *J* = 8.4 Hz, 1H), 6.75 (d, *J* = 8.4 Hz, 2H), 3.76 (s, 6H), 3.66 (m, 1H), 2.21 (br s, 1H), 2.15 (br s, 1H), 1.63–1.37 (m, 5H), 1.16–0.99 (m, 3H). ¹³C NMR (CD₃OD) δ (ppm) 165.11, 164.82, 159.28, 133.97, 133.00, 124.01, 122.33, 115.79, 105.34, 56.59, 53.91, 43.80, 40.38, 37.06, 36.28, 29.28, 27.54. LRMS (ES⁺): *m/z* 385 [M + H]⁺. HRMS (ES⁺): calcd for C₂₀H₂₅N₄O₄ [M + H]⁺ 385.1870, found 385.1857.

4-(2,6-Dimethoxybenzamido)-N-morpholino-1H-pyrazole-3-carboxamide (9f). Yield: 34 mg (solid), 53%. ¹H NMR (DMSO-*d*₆) δ (ppm) 13.30 (s, 1H), 9.66 (s, 1H), 9.55 (s, 1H), 8.31 (s, 1H), 7.39 (t, *J* = 8.4 Hz, 1H), 6.75 (d, *J* = 8.6 Hz, 2H), 3.76 (s, 6H), 3.62 (m, 4H), 2.84 (m, 4H). ¹³C NMR (DMSO-*d*₆) δ (ppm) 161.26, 161.18, 156.93, 131.41, 131.10, 122.90, 119.80, 115.01, 104.32, 65.98, 55.82, 54.31. LRMS (ES⁺): *m/z* 376 [M + H]⁺. HRMS (ES⁺): calcd for C₁₇H₂₂N₅O₅ [M + H]⁺ 376.1615, found 376.1620.

4-(2,6-Dimethoxybenzamido)-N-(3-(dimethylamino)propyl)-1H-pyrazole-3-carboxamide (9g). Yield: 41 mg (solid), 63%. ¹H NMR (DMSO-*d*₆) δ (ppm) 13.15 (brs, 1H), 9.70 (s, 1H), 8.99 (t, *J* = 6.3 Hz, 1H), 8.32 (s, 1H), 7.38 (t, *J* = 8.4 Hz, 1H), 7.31–7.29 (m, 4H), 7.22 (m, 1H), 6.74 (d, *J* = 8.4 Hz, 2H), 4.41 (d, *J* = 6.4 Hz, 2H), 3.75 (s, 6H). ¹³C NMR (DMSO-*d*₆) δ (ppm) 163.46, 161.29, 156.93, 139.45, 131.95, 131.10, 128.21, 127.26, 126.71, 122.58, 120.18, 115.01, 104.32, 55.82, 41.66. LRMS (ES⁺): *m/z* 381 [M + H]⁺. HRMS (ES⁺): calcd for C₂₀H₂₁N₄O₄ [M + H]⁺ 381.1557, found 381.1543.

4-(2,6-Dimethoxybenzamido)-N-(pyridin-2-ylmethyl)-1H-pyrazole-3-carboxamide (9h). Yield: 28 mg (solid), 42%. ¹H NMR (DMSO-*d*₆) δ (ppm) 13.33 (br s, 1H), 9.66 (s, 1H), 8.96 (t, *J* = 5.9, 1H), 8.50 (m, 1H), 8.34 (s, 1H), 7.74 (td, *J* = 7.7, 1.9 Hz, 1H), 7.39 (t, *J* = 8.4 Hz, 1H), 7.30 (d, *J* = 7.8 Hz, 1H), 7.25 (m, 1H), 6.73 (d, *J* = 8.4 Hz, 2H), 4.53 (d, *J* = 5.6 Hz, 2H), 3.75 (s, 6H). ¹³C NMR (DMSO-*d*₆) δ (ppm) 163.65, 161.32, 158.14, 156.93, 148.75, 136.68, 131.89, 131.10, 122.61, 122.06, 120.84, 120.18, 114.98, 104.32, 55.82, 43.54. LRMS (ES⁺): *m/z* 382 [M + H]⁺.

4-(2,6-Dimethoxybenzamido)-N-((3-methylpyridin-2-yl)methyl)-1H-pyrazole-3-carboxamide (9i). Yield: 30 mg (solid), 44%. ¹H NMR (DMSO-*d*₆) δ (ppm) 13.30 (br s, 1H), 9.68 (s, 1H), 8.72 (t, *J* = 5.0 Hz, 1H), 8.39 (d, *J* = 5.0 Hz, 1H), 8.34 (s, 1H), 7.60 (d, *J* = 7.6 Hz, 1H), 7.39 (t, *J* = 8.4 Hz, 1H), 7.23 (dd, *J* = 7.6, 5.0 Hz, 1H), 6.75 (d, *J* = 8.4 Hz, 2H), 4.54 (d, *J* = 5.0 Hz, 2H), 3.76 (s, 6H), 2.29 (s, 3H). ¹³C NMR (DMSO-*d*₆) δ (ppm) 163.28, 161.29, 156.96, 153.98, 145.81, 137.64, 132.10, 131.13, 130.64, 122.47, 122.24, 120.04, 114.98, 104.32, 55.84, 40.96, 17, 13. LRMS (ES⁺): *m/z* 396 [M + H]⁺. HRMS (ES⁺): calcd for C₂₀H₂₂N₅O₄ [M + H]⁺ 396.1666, found 396.1656.

N-(Cyclohexylmethyl)-4-(2,6-dimethoxybenzamido)-1H-pyrazole-3-carboxamide (9j). Yield: 56 mg (solid), 84%. ¹H NMR (CD₃OD) δ (ppm) 8.35 (s, 1H), 7.37 (t, *J* = 8.4 Hz, 1H), 6.71 (d, *J* = 8.4 Hz, 2H), 3.82 (s, 6H), 3.17 (d, *J* = 7.0 Hz, 2H), 1.77–1.64 (m, 5H), 1.55 (m, 1H), 1.28–1.13 (m, 3H), 1.00–0.89 (m, 2H). ¹³C NMR (CD₃OD) δ (ppm) 165.64, 165.00, 159.22, 134.15, 132.99, 123.89, 122.10, 115.69, 105.31, 56.58, 46.09, 39.42, 32.00, 27.57, 27.03. LRMS (ES⁺): *m/z* 386 [M + H]⁺. HRMS (ES⁺): calcd for C₂₀H₂₇N₄O₄ [M + H]⁺ 387.2027, found 387.2008.

4-(2,6-Dimethoxybenzamido)-N-phenyl-1H-pyrazole-3-carboxamide (9k). Yield: 48 mg (solid), 76%. ¹H NMR (DMSO-*d*₆) δ (ppm) 13.51 (s, 1H), 10.31 (s, 1H), 9.65 (s, 1H), 8.40 (s, 1H), 7.78 (d, *J* = 7.7 Hz, 2H), 7.41 (t, *J* = 8.5 Hz, 1H), 7.31 (t, *J* = 7.8 Hz, 2H), 7.09 (t, *J* = 7.3 Hz, 1H), 6.76 (d, *J* = 8.5 Hz, 2H), 3.77 (s, 6H). ¹³C NMR (DMSO-*d*₆) δ (ppm) 162.29, 161.40, 157.02, 138.10, 132.32, 131.19, 128.49, 123.81, 123.02, 120.69, 120.37, 114.98, 104.40, 55.88. LRMS (ES⁺): *m/z* 367 [M + H]⁺. HRMS (ES⁺): calcd for C₁₉H₁₉N₄O₄ [M + H]⁺ 367.1401, found 367.1402.

4-(2,6-Dimethoxybenzamido)-N-(pyridin-4-yl)-1H-pyrazole-3-carboxamide (9l). Yield: 10 mg (solid), 16%. ¹H NMR (DMSO-*d*₆) δ (ppm) 13.63 (s, 1H), 10.73 (s, 1H), 9.55 (s, 1H), 8.43 (d, *J* = 6.4 Hz, 3H), 7.83 (d, *J* = 5.5 Hz, 2H), 7.42 (t, *J* = 8.3 Hz, 1H), 6.77 (d, *J* = 8.4 Hz, 2H), 3.78 (s, 6H). LRMS (ES⁺): *m/z* 368 [M + H]⁺. HRMS (ES⁺): calcd for C₁₈H₁₈N₅O₄ [M + H]⁺ 368.1353, found 368.1347.

4-(2,6-Dimethoxybenzamido)-N-(pyridin-2-yl)-1H-pyrazole-3-carboxamide (9m). Yield: 10 mg (solid), 16%. ¹H NMR (DMSO-*d*₆) δ (ppm) 13.61 (s, 1H), 9.63 (s, 1H), 9.49 (s, 1H), 8.42 (s, 1H), 8.38 (br d, *J* = 4.6 Hz, 1H), 8.09 (d, *J* = 8.4 Hz, 1H), 7.83 (m, 1H), 7.42 (t, *J* = 8.4 Hz, 1H), 7.18 (m, 1H), 6.77 (d, *J* = 8.5 Hz, 2H), 3.78 (s, 6H). ¹³C NMR (DMSO-*d*₆) δ (ppm) 161.87, 161.55, 157.01, 150.45, 148.29, 138.41, 131.62, 131.30, 123.04, 120.90, 120.15, 114.66, 113.86, 104.35, 55.84. LRMS (ES⁺): *m/z* 368 [M + H]⁺. HRMS (ES⁺): calcd for C₁₈H₁₈N₅O₄ [M + H]⁺ 368.1335, found 368.1335.

4-(2,6-Dimethoxybenzamido)-N-((1*r*,4*r*)-4-hydroxycyclohexyl)-1H-pyrazole-3-carboxamide (9n). Yield: 51 mg (solid), 77%. ¹H NMR (DMSO-*d*₆) δ (ppm) 13.21 (br s, 1H), 9.75 (s, 1H), 8.28 (s, 1H), 8.09 (d, *J* = 8.4 Hz, 1H), 7.39 (t, *J* = 8.4 Hz, 1H), 6.75 (d, *J* = 8.4 Hz, 2H), 4.53 (br d, *J* = 3.8 Hz, 1H), 3.76 (s, 6H), 3.66 (m, 1H), 3.40–3.33 (m, 1H), 1.82 (m, 2H), 1.73 (m, 2H), 1.44 (m, 2H), 1.19 (m, 2H). ¹³C NMR (DMSO-*d*₆) 162.67, 161.25, 156.91, 131.07, 122.56, 115.10, 104.32, 68.11, 55.82, 47.00, 34.19, 30.00. LRMS (ES⁺): *m/z* 389 [M + H]⁺. HRMS (ES⁺): calcd for C₁₉H₂₃N₄O₅ [M + H]⁺ 389.1819, found 389.1800.

cis-trans-(4-(2,6-Dimethoxybenzamido)-N-(4-methylcyclohexyl)-1H-pyrazole-3-carboxamide (9o). Yield: 49 mg (solid), 74%. ¹H NMR (CD_3OD) δ (ppm) 8.36 (s, 0.5H), 8.33 (s, 0.5H), 7.39 (t, J = 8.5 Hz, 1H), 6.73 (d, J = 8.5 Hz, 2H), 4.05 (m, 0.5H), 3.84 (s, 6H), 3.76 (m, 0.5H), 1.96–1.32 (m, 8H), 1.06 (m, 1H), 0.98 (d, J = 6.5 Hz, 1.5 H), 0.92 (d, J = 6.6 Hz, 1.5H). ¹³C NMR (CD_3OD) δ (ppm) 165.06, 165.02, 164.76, 164.64, 159.25, 134.07, 134.01, 132.97, 123.99, 123.91, 122.30, 122.12, 115.70, 115.66, 105.39, 105.29, 56.54, 49.52, 46.86, 35.15, 33.67, 33.12, 31.53, 31.01, 30.09, 22.63, 21.25. LRMS (ES⁺): m/z 387 [M + H]⁺. HRMS (ES⁺): calcd for $\text{C}_{20}\text{H}_{27}\text{N}_4\text{O}_4$ [M + H]⁺ 387.2027, found 387.2007.

tert-Butyl 4-(4-(2,6-Dimethoxybenzamido)-1H-pyrazole-3-carboxamido)piperidine-1-carboxylate (9p). Yield: 50 mg (solid), 41%. ¹H NMR (CD_3OD) δ (ppm) 8.35 (s, 1H), 7.37 (t, J = 8.4 Hz, 1H), 6.71 (d, J = 8.4 Hz, 2H), 4.08–3.99 (m, 3H), 3.82 (s, 6H), 2.90 (m, 2H), 1.89 (m, 2H), 1.51 (m, 2H), 1.46 (s, 9H). ¹³C NMR (CD_3OD) δ (ppm) 165.00, 164.89, 159.22, 156.39, 134.00, 132.99, 124.03, 122.16, 115.72, 105.35, 81.17, 56.61, 47.67, 44.39, and 43.61 (br d, rotamers), 32.69, 28.79. LRMS (ES⁺): m/z 474 [M + H]⁺. HRMS (ES⁺): calcd for $\text{C}_{23}\text{H}_{32}\text{N}_5\text{O}_6$ [M + H]⁺ 474.2347, found 474.2324.

N-(1-Benzylpyrrolidin-3-yl)-4-(2,6-dimethoxybenzamido)-1H-pyrazole-3-carboxamide (9q). Yield: 69 mg (solid), 89%. ¹H NMR (CD_3OD) δ (ppm) 8.32 (s, 1H), 7.36 (t, J = 8.4 Hz, 1H), 7.32–7.22 (m, 5H), 6.68 (d, J = 8.4 Hz, 2H), 4.52 (m, 1H), 3.78 (s, 6H), 3.58 (d, J = 2.5 Hz, 2H), 2.76 (m, 2H), 2.58 (dd, J = 10.0, 4.3, 1H), 2.43 (q, J = 8.1 Hz, 1H), 2.27 (m, 1H), 1.75 (m, 1H). ¹³C NMR (CD_3OD) δ (ppm) 165.06, 165.00, 159.22, 139.26, 133.92, 132.99, 130.33, 129.50, 128.49, 124.01, 122.16, 115.67, 105.32, 61.26, 61.17, 56.58, 53.83, 49.19, 32.54. LRMS (ES⁺): m/z 450 [M + H]⁺. HRMS (ES⁺): calcd for $\text{C}_{24}\text{H}_{28}\text{N}_5\text{O}_4$ [M + H]⁺ 450.2136, found 450.2113.

4-(2,6-Dimethoxybenzamido)-N-(2-methoxyethyl)-1H-pyrazole-3-carboxamide (9r). Yield: 39 mg (solid), 65%. ¹H NMR (CD_3OD) δ (ppm) 8.35 (s, 1H), 7.38 (t, J = 8.4 Hz, 1H), 6.72 (d, J = 8.4 Hz, 2H), 3.83 (s, 6H), 3.53 (s, 4H), 3.37 (s, 3H). ¹³C NMR (CD_3OD) δ (ppm) 165.76, 165.05, 159.26, 134.10, 132.99, 115.71, 105.32, 72.07, 59.03, 56.56, 39.52. LRMS (ES⁺): m/z 349 [M + H]⁺. HRMS (ES⁺): calcd for $\text{C}_{16}\text{H}_{21}\text{N}_4\text{O}_5$ [M + H]⁺ 349.1506, found 349.1504.

4-(2,6-Dimethoxybenzamido)-N-pentyl-1H-pyrazole-3-carboxamide (9s). Yield: 52 mg (solid), 84%. ¹H NMR ($\text{DMSO}-d_6$) δ (ppm) 13.23 (br s, 1H), 9.74 (s, 1H), 8.38 (br s, 1H), 8.29 (s, 1H), 7.39 (t, J = 8.5 Hz, 1H), 6.75 (d, J = 8.5 Hz, 2H), 3.76 (s, 6H), 3.19 (m, 2H), 1.49 (quint, J = 7.2 Hz, 2H), 1.31–1.22 (m, 4H), 0.85 (t, J = 7.0 Hz, 3H). ¹³C NMR ($\text{DMSO}-d_6$) δ (ppm) 163.39, 161.20, 156.93, 132.25, 131.07, 122.35, 119.79, 115.05, 104.32, 55.82, 37.95, 28.77, 28.57, 21.78, 13.87. LRMS (ES⁺): m/z 361 [M + H]⁺. HRMS (ES⁺): calcd for $\text{C}_{18}\text{H}_{25}\text{N}_4\text{O}_4$ [M + H]⁺ 361.1870, found 361.1868.

4-(2,6-Dimethoxybenzamido)-N-(3-isopropoxypropyl)-1H-pyrazole-3-carboxamide (9t). Yield: 64 mg (solid), 95%. ¹H NMR (CD_3OD) δ (ppm) 8.35 (s, 1H), 7.38 (t, J = 8.5 Hz, 1H), 6.71 (d, J = 8.5 Hz, 2H), 3.83 (s, 6H), 3.58 (sept, J = 6.1 Hz, 1H), 3.53 (t, J = 6.1 Hz, 2H), 3.45 (t, J = 6.6 Hz, 2H), 1.83 (quin, J = 6.4 Hz, 2H), 1.15 (d, J = 6.1 Hz, 6H). ¹³C NMR (CD_3OD) δ (ppm) 165.58, 165.00, 159.22, 134.17, 132.99, 123.82, 121.99, 115.69, 105.32, 73.08, 67.50, 56.61, 38.06, 30.72, 22.49. LRMS (ES⁺): m/z 391 [M + H]⁺. HRMS (ES⁺): calcd for $\text{C}_{19}\text{H}_{27}\text{N}_4\text{O}_5$ [M + H]⁺ 391.1976, found 391.1961.

4-(2,6-Dimethoxybenzamido)-N-(3-(dimethylamino)propyl)-1H-pyrazole-3-carboxamide (9u). Yield: 49 mg (solid), 76%. ¹H NMR (CD_3OD) δ (ppm) 8.23 (s, 1H), 7.26 (t, J = 8.4 Hz, 1H), 6.59 (d, J = 8.4 Hz, 2H), 3.71 (s, 6H), 3.26 (t, J = 7.5 Hz, 2H), 2.26 (t, J = 7.5 Hz, 2H), 2.11 (s, 6H), 1.65 (q, J = 7.5 Hz, 2H). ¹³C NMR (CD_3OD) δ (ppm) 165.70, 164.94, 159.22, 134.15, 132.99, 123.92, 122.05, 115.75, 105.35, 58.25, 56.61, 45.52, 38.23, 28.32. LRMS (ES⁺): m/z 376 [M + H]⁺. HRMS (ES⁺): calcd for $\text{C}_{18}\text{H}_{26}\text{N}_5\text{O}_4$ [M + H]⁺ 376.1979, found 376.1965.

4-(2,6-Dimethoxybenzamido)-N-(2-(pyrrolidin-1-yl)ethyl)-1H-pyrazole-3-carboxamide (9v). Yield: 57 mg (solid), 86%. ¹H NMR (CD_3OD) δ (ppm) 8.34 (s, 1H), 7.38 (t, J = 8.4 Hz, 1H), 6.71 (d, J = 8.4 Hz, 2H), 3.83 (s, 6H), 3.51 (t, J = 6.9 Hz, 2H), 2.69 (t, J = 6.9 Hz, 2H), 2.59 (m, 4H), 1.80 (m, 4H). ¹³C NMR (CD_3OD) δ (ppm) 165.69, 164.97, 159.22, 134.09, 132.99, 123.89, 122.01, 115.72, 105.32,

56.58, 56.32, 55.08, 38.64, 24.31. LRMS (ES⁺): m/z 388 [M + H]⁺. HRMS (ES⁺): calcd for $\text{C}_{19}\text{H}_{26}\text{N}_5\text{O}_4$ [M + H]⁺ 388.1979, found 388.1965.

4-(2,6-Dimethoxybenzamido)-N-(2-morpholinoethyl)-1H-pyrazole-3-carboxamide (9w). Yield: 37 mg (solid), 53%. ¹H NMR (CD_3OD) δ (ppm) 8.34 (s, 1H), 7.40 (t, J = 8.4 Hz, 1H), 6.73 (d, J = 8.4 Hz, 2H), 3.84 (s, 6H), 3.70 (t, J = 4.5 Hz, 4H), 3.5 (t, J = 6.6, 2H), 2.57 (t, J = 6.6 Hz, 2H), 2.52 (br t, J = 4.5 Hz, 4 Hz). ¹³C NMR (CD_3OD) δ (ppm) 165.67, 165.00, 159.23, 134.06, 132.96, 123.86, 122.02, 115.72, 105.32, 67.80, 58.60, 56.55, 54.67, 36.50. LRMS (ES⁺): m/z 404 [M + H]⁺. HRMS (ES⁺): calcd for $\text{C}_{19}\text{H}_{26}\text{N}_5\text{O}_5$ [M + H]⁺ 404.1928, found 404.1929.

■ ASSOCIATED CONTENT

■ Supporting Information

Kinase profiling of **4f**, **4m**, **4y**, and **9g** against a panel of mammalian kinases; calculated physicochemical properties of all synthesized aminopyrazole derivatives (PDF and PDB). This material is available free of charge via the Internet at <http://pubs.acs.org>.

■ AUTHOR INFORMATION

Corresponding Authors

*For P.G.W.: phone, +44 (0)1382 386231; e-mail, p.g.wyatt@dundee.ac.uk.

*For R.B.: e-mail, brenk@uni-mainz.de.

Present Address

[§]Johannes Gutenberg-Universität Mainz Institut für Pharmazie und Biochemie Staudinger Weg 5 D-55128 Mainz, Germany

Notes

The authors declare no competing financial interest.

■ ACKNOWLEDGMENTS

We thank the Wellcome Trust (grant 077705 and strategic award WT083481) for financial support for these studies. We also thank Iain Collie, Irene Hallyburton, and Bhavya Rao for carrying out the *T. b. brucei* and MRC5 proliferation studies, Daniel James for data management, and Gina McKay for performing HRMS analyses and for assistance with performing other NMR and MS analyses.

■ ABBREVIATIONS USED

GSK, glycogen synthase kinase; HAT, human African trypanosomiasis; CDK, cyclin dependent kinase; *T. brucei*, *Trypanosoma brucei*; *T. b. brucei*, *Trypanosoma brucei brucei*; SAR, structure–activity relationships; PK, protein kinase

■ REFERENCES

- Pink, R.; Hudson, A.; Mouries, M. A.; Bendig, M. Opportunities and challenges in antiparasitic drug discovery. *Nature Rev. Drug Discovery* **2005**, *4*, 727–740.
- Walton, J. G.; Jones, D. C.; Kiuru, P.; Durie, A. J.; Westwood, N. J.; Fairlamb, A. H. Synthesis and Evaluation of Indatraline-Based Inhibitors for Trypanothione Reductase. *ChemMedChem* **2011**, *6*, 321–328.
- Fairlamb, A. H. Chemotherapy of human African trypanosomiasis: current and future prospects. *Trends Parasitol.* **2003**, *19*, 488–494.
- Alsfeld, S.; Eckert, S.; Baker, N.; Glover, L.; Sanchez-Flores, A.; Leung, K. F.; Turner, D. J.; Field, M. C.; Berrian, M.; Horn, D. High-throughput decoding of antitrypanosomal drug efficacy and resistance. *Nature* **2012**, *482*, 232–236.
- Allocco, J. J.; Donald, R.; Zhong, T.; Lee, A.; Tang, Y. S.; Hendrickson, R. C.; Liberator, P.; Nare, B. Inhibitors of casein kinase 1

- block the growth of *Leishmania major* promastigotes in vitro. *Int. J. Parasitol.* **2006**, *36*, 1249–1259.
- (6) Alsford, S.; Turner, D. J.; Obado, S. O.; Sanchez-Flores, A.; Glover, L.; Berriman, M.; Hertz-Fowler, C.; Horn, D. High-throughput phenotyping using parallel sequencing of RNA interference targets in the African trypanosome. *Genome Res.* **2011**, *21*, 915–924.
- (7) Jones, N. G.; Thomas, E. B.; Brown, E.; Dickens, N. J.; Hammarton, T. C.; Mottram, J. C. Regulators of *Trypanosoma brucei* cell cycle progression and differentiation identified using a kinome-wide RNAi screen. *PLoS Pathog.* **2014**, *10*, e1003886.
- (8) Naula, C.; Parsons, M.; Mottram, J. C. Protein kinases as drug targets in trypanosomes and Leishmania. *Biochim. Biophys. Acta* **2005**, *1754*, 151–159.
- (9) Barquilla, A.; Saldivia, M.; Diaz, R.; Bart, J.-M.; Vidal, I.; Calvo, E.; Hall, M. N.; Navarro, M. Third target of rapamycin complex negatively regulates development of quiescence in *Trypanosoma brucei*. *Proc. Natl. Acad. Sci. U. S. A.* **2012**, *109*, 14399–14404.
- (10) Domenicali Pfister, D.; Burkard, G.; Morand, S.; Renggli, C. K.; Roditi, I.; Vassella, E. A Mitogen-activated protein kinase controls differentiation of bloodstream forms of *Trypanosoma brucei*. *Eukaryotic Cell* **2006**, *5*, 1126–1135.
- (11) Mony, B. M.; MacGregor, P.; Ivens, A.; Rojas, F.; Cowton, A.; Young, J.; Horn, D.; Matthews, K. Genome-wide dissection of the quorum sensing signalling pathway in *Trypanosoma brucei*. *Nature* **2014**, *505*, 681–685.
- (12) Vassella, E.; Kramer, R.; Turner, C. M.; Wankell, M.; Modes, C.; van den Bogaard, M.; Boshart, M. Deletion of a novel protein kinase with PX and FYVE-related domains increases the rate of differentiation of *Trypanosoma brucei*. *Mol. Microbiol.* **2001**, *41*, 33–46.
- (13) Ojo, K. K.; Gillespie, J. R.; Riechers, A. J.; Napuli, A. J.; Verlinde, C. L.; Buckner, F. S.; Gelb, M. H.; Domostoj, M. M.; Wells, S. J.; Scheer, A.; Wells, T. N.; Van Voorhis, W. C. Glycogen synthase kinase 3 is a potential drug target for African trypanosomiasis therapy. *Antimicrob. Agents Chemother.* **2008**, *52*, 3710–3717.
- (14) Hoeflich, K. P.; Luo, J.; Rubie, E. A.; Tsao, M. S.; Jin, O.; Woodgett, J. R. Requirement for glycogen synthase kinase-3beta in cell survival and NF-kappaB activation. *Nature* **2000**, *406*, 86–90.
- (15) Kugimiya, F.; Kawaguchi, H.; Ohba, S.; Kawamura, N.; Hirata, M.; Chikuda, H.; Azuma, Y.; Woodgett, J. R.; Nakamura, K.; Chung, U. I. GSK-3beta controls osteogenesis through regulating Runx2 activity. *PLoS One* **2007**, *2*, e837.
- (16) Khanfar, M. A.; Hill, R. A.; Kaddoumi, A.; El Sayed, K. A. Discovery of novel GSK-3beta inhibitors with potent in vitro and in vivo activities and excellent brain permeability using combined ligand- and structure-based virtual screening. *J. Med. Chem.* **2010**, *53*, 8534–8545.
- (17) Meijer, L.; Flajolet, M.; Greengard, P. Pharmacological inhibitors of glycogen synthase kinase 3. *Trends Pharmacol. Sci.* **2004**, *25*, 471–480.
- (18) Uno, Y.; Iwashita, H.; Tsukamoto, T.; Uchiyama, N.; Kawamoto, T.; Kori, M.; Nakanishi, A. Efficacy of a novel, orally active GSK-3 inhibitor 6-Methyl-N-[3-[[3-(1-methylethoxy)propyl]-carbamoyl]-1H-pyrazol-4-yl]pyridine-3-carboxamide in tau transgenic mice. *Brain Res.* **2009**, *1296*, 148–163.
- (19) Wyatt, P. G.; Woodhead, A. J.; Berdini, V.; Boulstridge, J. A.; Carr, M. G.; Cross, D. M.; Davis, D. J.; Devine, L. A.; Early, T. R.; Feltell, R. E.; Lewis, E. J.; McMenamin, R. L.; Navarro, E. F.; O'Brien, M. A.; O'Reilly, M.; Reule, M.; Saxty, G.; Seavers, L. C.; Smith, D. M.; Squires, M. S.; Trewartha, G.; Walker, M. T.; Woolford, A. J. Identification of *N*-(4-piperidinyl)-4-(2,6-dichlorobenzoylamino)-1H-pyrazole-3-carboxamide (AT7519), a novel cyclin dependent kinase inhibitor using fragment-based X-ray crystallography and structure based drug design. *J. Med. Chem.* **2008**, *51*, 4986–4999.
- (20) Wyatt, P. G.; Berdini, V.; Gill, A. L.; Trewartha, G.; Woodhead, A. J.; Navarro, E. F.; O'Brien, M. A.; Phillips, T. R. Preparation of pyrazole derivatives for use in pharmaceutical compositions for the inhibition of cyclin dependent kinases and glycogen synthase kinases. Patent Application WO2006077419 A1, 2006.
- (21) Hofer, A.; Ekanem, J. T.; Thelander, L. Allosteric regulation of *Trypanosoma brucei* ribonucleotide reductase studied in vitro and in vivo. *J. Biol. Chem.* **1998**, *273*, 34098–34104.
- (22) Urbaniak, M. D.; Mathieson, T.; Bantscheff, M.; Eberhard, D.; Grimaldi, R.; Miranda-Saavedra, D.; Wyatt, P.; Ferguson, M. A.; Frearson, J.; Drewes, G. Chemical proteomic analysis reveals the druggability of the kinome of *Trypanosoma brucei*. *ACS Chem. Biol.* **2012**, *7*, 1858–1865.
- (23) Oduor, R. O.; Ojo, K. K.; Williams, G. P.; Bertelli, F.; Mills, J.; Maes, L.; Pryde, D. C.; Parkinson, T.; Van Voorhis, W. C.; Holler, T. P. *Trypanosoma brucei* glycogen synthase kinase-3, a target for anti-trypanosomal drug development: a public–private partnership to identify novel leads. *PLoS Negl. Trop. Dis.* **2011**, *5*, e1017.
- (24) Ojo, K. K.; Arakaki, T. L.; Napuli, A. J.; Inampudi, K. K.; Keyloun, K. R.; Zhang, L.; Hol, W. G.; Verlinde, C. L.; Merritt, E. A.; Van Voorhis, W. C. Structure determination of glycogen synthase kinase-3 from *Leishmania major* and comparative inhibitor structure–activity relationships with *Trypanosoma brucei* GSK-3. *Mol. Biochem. Parasitol.* **2011**, *176*, 98–108.
- (25) Woodland, A.; Grimaldi, R.; Luksch, T.; Cleghorn, L. A.; Ojo, K. K.; Van Voorhis, W. C.; Brenk, R.; Frearson, J. A.; Gilbert, I. H.; Wyatt, P. G. From on-target to off-target activity: identification and optimization of *Trypanosoma brucei* GSK3 inhibitors and their characterisation as anti-*Trypanosoma brucei* drug discovery lead molecules. *ChemMedChem* **2013**, *8*, 1127–1137.
- (26) Thompson, J. D.; Higgins, D. G.; Gibson, T. J. CLUSTAL W: improving the sensitivity of progressive multiple sequence alignment through sequence weighting, position-specific gap penalties and weight matrix choice. *Nucleic Acids Res.* **1994**, *22*, 4673–4680.
- (27) Sali, A.; Blundell, T. L. Comparative protein modelling by satisfaction of spatial restraints. *J. Mol. Biol.* **1993**, *234*, 779–815.
- (28) Rarey, M.; Kramer, B.; Lengauer, T.; Klebe, G. A fast flexible docking method using an incremental construction algorithm. *J. Mol. Biol.* **1996**, *261*, 470–489.
- (29) Gong, L.; Hirschfeld, D.; Tan, Y. C.; Heather Hogg, J.; Peltz, G.; Avnur, Z.; Dunten, P. Discovery of potent and bioavailable GSK-3beta inhibitors. *Bioorg. Med. Chem. Lett.* **2010**, *20*, 1693–1696.
- (30) *The PyMOL Molecular Graphics System*, Version 0.99; Schrödinger, LLC.
- (31) Eastwood, B. J.; Farmen, M. W.; Iversen, P. W.; Craft, T. J.; Smallwood, J. K.; Garbison, K. E.; Delapp, N. W.; Smith, G. F. The minimum significant ratio: a statistical parameter to characterize the reproducibility of potency estimates from concentration-response assays and estimation by replicate-experiment studies. *J. Biomol. Screening* **2006**, *11*, 253–261.
- (32) Bain, J.; Plater, L.; Elliott, M.; Shpiro, N.; Hastie, C. J.; McLauchlan, H.; Klevernic, I.; Arthur, J. S.; Alessi, D. R.; Cohen, P. The selectivity of protein kinase inhibitors: a further update. *Biochem. J.* **2007**, *408*, 297–315.
- (33) Raz, B.; Iten, M.; Grether-Buhler, Y.; Kaminski, R.; Brun, R. The Alamar Blue assay to determine drug sensitivity of African trypanosomes (*T. b. rhodesiense* and *T. b. gambiense*) in vitro. *Acta Trop.* **1997**, *68*, 139–147.